Aerospace Science and Technology 141 (2023) 108537

Contents lists available at ScienceDirect

Aerospace Science and Technology

journal homepage: www.elsevier.com/locate/aescte

On-field noise measurements and acoustic characterisation of multi-rotor small unmanned aerial systems

Carlos Ramos-Romero [a,*], Nathan Green [a], Antonio J. Torija [a], César Asensio [b]

[a] Acoustics Research Centre, University of Salford, 43 Crescent, Salford, Manchester, M5 4WT, United Kingdom
[b] ETSI Sistemas de Telecomunicación, Departamento de Ingeniería Audiovisual y Comunicaciones, Grupo de Investigación en Instrumentación y Acústica Aplicada (I2A2), Universidad Politécnica de Madrid, C. Nikola Tesla, Madrid, 28031, Spain

ARTICLE INFO

Article history:
Received 2 March 2023
Received in revised form 20 July 2023
Accepted 24 July 2023
Available online 2 August 2023
Communicated by Damiano Casalino

Keywords:
sUAS
Drone noise
Noise regulations
Noise metrics
Sound quality metrics
On-field noise measurements

ABSTRACT

The noise signature of small Unmanned Aerial Systems (sUAS) is highly influenced by specific operating and weather conditions. Accurate noise assessment of sUAS operations requires field noise measurements that capture all the complexity of sound emission and propagation during realistic flight situations. This paper presents a measurement and analysis framework for the acoustic characterisation of sUAS through the calculation of conventional noise metrics (L_{Amax} and L_{AE}), frequency and directivity features. Using a multi-channel measurement approach, and back-propagating the sound from ground microphone to source, the presented framework allows the calculation of acoustic hemispheres for a selection of acoustic metrics. Important findings are that *(i)* the framework is robust for a variety of multi-rotor sUAS varying in size and configuration; *(ii)* broadband noise and tonal noise are the dominant noise sources during flyover for larger sUAS and smaller sUAS respectively; *(iii)* the maximum noise radiation of the sUAS tested is found in the rear arc of polar directivity; and *(iv) angles of maximum radiation of amplitude modulated noise have been found for most sUAS tested at* Θ *angles* $\pm 30°$. This work is intended to be relevant in establishing common protocols regarding sUAS acoustic certification between environmental policymakers, stakeholders, and industry.

1. Introduction

In recent years, research on Unmanned Aircraft Systems (UAS) noise has attracted extensive interest due to the impact of the noise generated on exposed communities [1]. Small UAS (sUAS), classed as aircraft with a maximum Takeoff weight of 25 kg (or 55 lb) according to the US Federal Aviation Administration [2], European Aviation Safety Agency (EASA) [3] and UK Civil Aviation Authority [4], are of significant interest for industry due to their unlimited innovative applications for sectors such as aerospace, logistics, transport, and environmental monitoring [5].

Previous research has suggested sUAS are perceived as more annoying than road vehicles and conventional aircraft, at the same sound level [6,7]. This is thought to be due to the unconventional noise signature of sUAS, with high tonal and high-frequency content [7,8], but also due to their specific operational procedures, such as "loitering" effect due to flying in close proximity to the ground [6]. This has led to noise to be identified as one of the main barriers for public acceptance of sUAS operations [9,10].

Working towards sUAS noise assessment, the first step is to have a method for the accurate acoustic characterisation of these vehicles operating under realistic flight conditions. There have been considerable efforts to understand the noise emission of sUAS [11]. The focus has been mainly on propeller-driven sUAS, with several studies on single propellers [12,13], dual propellers ([14]) and multi-rotor configurations [15]. These studies have been conducted under static conditions in an anechoic chamber. Studies on multi-rotor configurations have also been conducted in a wind tunnel [16] to simulate forward flight conditions, and a large anechoic chamber with the vehicle flying over a microphone array [17].

Several field studies, measuring the noise emission of sUAS under real operation conditions have also been conducted. Schäffer et al. [11] provide a review of field studies for sUAS noise measurement, including measured noise values for a series of multi-rotors both in hover and forward flight. Field measurements present important challenges, as measured noise signals might be influenced by ground effects and weather conditions [17]. Alexander et al. [18] found that wind speed has a significant impact on measured broadband and tonal noise. Other potential issues are reduced signal-to-noise ratio, and signal contamination due to the presence of other sound sources. However, field measurements are essential

* Corresponding author.
E-mail address: c.a.ramosromero@salford.ac.uk (C. Ramos-Romero).

https://doi.org/10.1016/j.ast.2023.108537

Nomenclature

L_W	Sound power level
L_p	Sound pressure level
L_{Amax}	Maximum A-weighted sound pressure level
L_{AE}	A-weighted sound exposure level
L_{Aeq}	Equivalent continuous sound pressure level
L_{ground}	Sound level at ground microphone position
$L_{source}(r)$	Back-propagated sound level at radius r
σ_∇	Losses due to spherical spreading
σ_α	Losses due to atmospheric absorption
α	Atmospheric sound attenuation coefficient
σ_{ground}	Losses due to ground surface type
Θ	Horizontal angle
ϕ	Polar angle
t	Time
$d_{(\text{Drone,mic})}$	Drone-to-noise distance
d_x	sUAS position over flight path (x-axis)
d_{mic}	Microphone distance (y-axis)
h_{AGL}	Height above the ground level (z-axis)
OASPL	Overall A-weighted Sound Pressure Level
EPNL	Effective Perceived Noise Level
SQMs	Sound Quality Metrics
N_r	Number of rotors
N_b	Number of blades
TOW	Takeoff weight
ν	Flight speed
M	Mach Number
BPF	Blade Passing Frequency
f_0	Average Blade Passing Frequency
RPM	Revolutions per minute
RPS	Revolutions per second
D	Propeller diameter
J	Propeller advance ratio
$\overline{J}$	Average propeller advance ratio

to *(i)* understand the sound propagation from vehicle to receiver, under different atmospheric conditions; *(ii)* understand the directivity characteristics under different operating conditions; and *(iii)* computing time-integrated metrics such as Sound Exposure Level (L_{AE}) and Effective Perceived Noise Level (EPNL), based on a calculation window defined by the maximum sound level L_{Amax} - 10 dB. This information will be required to evaluate the noise footprints of sUAS for the evaluation of community noise impact.

This paper is presenting a method for the acoustic characterisation of sUAS under real flight conditions. The method has been derived from a dynamic noise emission characterisation previously applied to conventional rotorcraft operating under realistic scenarios [19]. Although developed with a focus on sUAS, the method is flexible to accommodate rotorcraft of different size. Compared to multirotor sUAS, with inflow non-perpendicular to the propeller disk [20], fixed-wing sUAS (mainly with axial flow) will have significantly different angles of maximum noise emission. The method presented will be able to compute noise metrics for both types of aircraft, but the different source directivity of each configuration and operation should be taken into account for the appropriate interpretation of the results. A potential limiting factor will be to ensure enough signal-to-noise ratio to compute acoustic metrics.

The method was formulated to compute noise emission hemispheres from the sUAS during flyover operations. These hemispheres, containing 3D directivity patterns, can be calculated for a number of energy-based noise metrics, including both broadband and tonal noise. To illustrate the applicability of the method, a comprehensive acoustic characterisation is presented for four types of multirotor sUAS with different size and number of rotors.

Since there is still no published standardised methodology for measuring the noise emitted by Unmanned Aerial Vehicles [21,22], the measuring set-up follows the up-to-date technical recommendations for outdoor tests from NASA's Technical Group [23] and the ISO/DIS 5305 [24]. However, the referenced documents do not provide further details about the post-processing of the measurement results.

The method presented comprises three main steps: *(i)* The description of the operational conditions of the sUAS, *(ii)* The acquisition of meteorological data and sUAS noise signals on the ground, and *(iii)* the analysis of the data in the time and frequency domain, for the acoustic characterisation of the flyover, the back-propagation of noise signals from ground to receiver and the hemisphere construction, containing directivity information. The method has also been extended for an aerodynamic scaling of the acoustic metrics, in terms of an average Advance Ratio of the sUAS, to generalise the results presented in the paper.

The remaining of the paper is organised as follows. Section 2 presents the context, including a description of the previous experimental considerations for on-field multi-rotor aircraft noise measurements. Section 3 describes the applied method used for the on-field acoustic data acquisition and further sUAS noise characterisation. Section 4 presents the results based on acoustic metrics and directivity plots over the microphone array and noise hemispheres. The main contributions and limitations of the applied methodology and potential future applications of its implementation are discussed in Section 5. Finally, the conclusions of this work are given in Section 6.

2. Background

Early research into the noise characterisation of conventional aircraft aimed to reporting both Sound Pressure Level (L_p) and sound directivity using different types of microphone arrays mounted in an inverted position on reflecting boards. Power Spectral Density (PSD) has also been generally reported, especially for understanding the noise emission of propeller-driven aircraft. Humphreys et al. [25] developed an extensive phased-array for aircraft propulsion and airframe noise flyover measurements, validating its performance with a hexacopter hovering to assess the potential application for sUAS noise measurement. Furthermore, alternative microphone array configurations have been designed with a reduced number of ground-mounted microphones for sUAS flyover detection [26,27].

Sound Level Meters (SLMs) have been another useful device for recording sUAS sound pressure levels. Although the number of channels is limited to a single microphone, their relatively simple operation and real-time signal processing capability have made these devices a standard tool for capturing the sUAS acoustic profile [28–30]. A comprehensive database of sUAS noise measurements was published by Senzig et al. [31], Senzig and Marsan [32] and Read et al. [33]. This database describes the results of three types of multirotor and one fixed-wing aircraft noise measurements. The study included a variety of sUAS manoeuvres such as hovering, flyover, take-off, landing and inspection manoeuvres.

Multichannel data acquisition systems have also been previously used within the data collection methodology for sUAS noise studies. Time-domain data post-processing allows for the calculation of more complex acoustic metrics such as L_{AE}, EPNL and

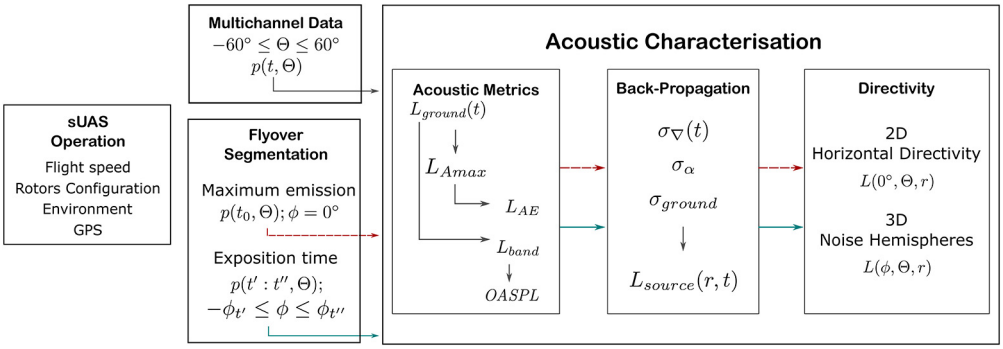

Fig. 1. Workflow for the sUAS acoustic characterisation.

Sound Quality Metrics (SQMs) [34–38]. Dedicated audio recording systems have also been applied to measure and characterise sUAS through the collection and analysis of both acoustic and SQMs [39].

More recent developments of robust ground-based acoustic measurement procedures building upon conventional aircraft noise measurement techniques have been developed, where multichannel ground plate-mounted microphone arrays and perpendicular flight paths have been utilised [33,40,41,35]. The summary of the detailed previous studies for on-field sUAS noise measurements is presented in Table 1.

Although, guidelines on noise measurement for UAS have been recently published by EASA, there is no agreement in standardised methods. For instance, EASA's guidelines require a measurement with a single microphone in an inverted position over a flat plate on the ground [42], while the technical recommendations for outdoor tests from NASA's Technical Group [23] are based on an 11-microphone array (inverted on a flat ground plate) to reconstruct the 3D directivity. In addition to this, there is a lack of standardised methods with guidance on *(i)* the post-processing and reporting of measured acoustic data; *(ii)* noise certification of sUAS, including operational procedures and assessment points; and *(iii)* sUAS noise limits.

3. Methods

The method allows the acoustic characterisation of sUAS during flyovers. Sound pressure levels are estimated at specific emission angles using noise measurements acquired by a linear microphone array on the ground. The meteorological conditions were monitored during the acoustic measurements.

The method has been designed to characterise the noise emission of sUAS under real flyover operations in terms of the sound pressure level emitted along a hemisphere whose centre coincides with the position of an equivalent point source that simulates the sUAS. The sound pressure hemispheres characterise the emissions in terms of sound pressure level, frequency spectra, and emission angle for a standardised distance r which, in this paper, has been considered to be 1 m. Furthermore, the performance of each multirotor system at different flyover conditions has been evaluated in terms of an average Advance Ratio.

Fig. 1 shows a flow diagram with an overall description of the method developed for sUAS acoustic characterisation. A detailed description of each step is provided in the remaining sub-sections of Section 3.

3.1. sUAS features and operations

The most common operations during sUAS acoustic studies are hovering, take-off, landing, and flyovers, as presented in Table 1. The flyover operation allows the measurement of the progressive changes of the acoustic signal associated with the approach/departure to/from fixed receivers. Although only flyover results are presented in this paper, the measurement campaign included different types of sUAS operations. The method presented in this paper will be extended in future efforts to account for hover, landing and take-off operations. A comprehensive acoustic dataset including hover, flyover, landing and take-off operations is available at [44].

The height above the ground level h_{AGL} for all the flyovers remained at 10 m during the tests. The same qualified pilot operated the four sUAS tested during the measurement campaign to avoid changes in the flight pattern due to pilot experience and competence. The operations were performed at different Take-off weights (TOW) depending on the payload set, see Table 2.

Flyovers of each sUAS were measured at fast and slow speeds that were set by the maximum and minimum programmable speed v without any change in the power setting during the straight-line overflights. The sUAS features and configuration of the tested sUAS are summarised in Table 2.

The test requirements in terms of sUAS flight conditions (i.e., positioning, height, and speed mainly) were controlled internally by the aircraft's own instruments. Unfortunately, the experimental team did not have access to a detailed record of GPS information; therefore, the calculations presented in this paper are based on the nominal data from the flight procedure, synchronising the sUAS location with the acoustic data from the audio recording itself. This added a certain level of uncertainty in the acoustic outputs presented in this paper. This opportunity for improvement will be included in future implementations to achieve a more accurate synchronisation of the acoustic data with the positioning of the sound source.

Site description

The sUAS noise measurements were carried out on a farm land located in Edzell, a village in Angus, Scotland, on the 17^{th}. of August 2022. This location is primarily used for the cultivation of feed for livestock. The terrain surfaces showed signs of recent harvest activities. The selected site was located sufficiently far from major noise sources, such as main roads, as is depicted in Fig. 2.

A linear array with nine 1/2 microphones placed in an inverted position over a ground plate was located over the North-South axis. The depicted points on this line represent the reference location for microphone 1 located towards North (mN), the array's central microphone 5 (mC) and microphone 9 located towards South (mS).

The sUAs flight path was perpendicular to the line of the microphones and passed exactly over the central microphone. Both points (ss1) and (ss2) represent the start/stop point of each flyover from ss1 to ss2 or the other way around. The position of the Meteorological station (M) and the Control and operations point (C) is also depicted on this layout.

Table 1
Previous experiments: On-field noise measurements and acoustic characterisation for small Unmanned Aerial Systems.

Author	Data Acquisition System	Acoustic Sensors		Reported acoustic metrics*	Test ground type	sUAS altitude AGL	sUAS type	sUAS operations*	Additional data
		Number	Description						
Humphreys et al. [25]	Multichannel data acquisition system	185	Field-Deployable electret Microphone Phased Array	SPL Z-weighting [dB] Source localisation.	Concrete Plastic ground plates	40 to 400 [ft]	Hexacopter	H	Video recorder Weather station
Kloet et al. [28]	SPL meters	2	1/2" free-field microphone: 2 SPL meter microphones	SPL, A-weighted [dB]	Grass	5, 10, 15, 20 [m]	Quadcopter	H	Anemometer
Zhang et al. [26]	Acoustic camera	40	Phased microphone array	PSD SPL Z-weighting [dB] Source localisation.	Concrete	2.1 to 30 [m]	Quadcopter	H, F	n.r.
Cabell et al. [43]; Zawodny et al. [35]; Christian and Cabell [34]	Multichannel	3	1/2" free-field microphones: 1 tripod-mounted mic 2 ground plane-mounted mics	SPL Z-weighting [dB] SEL A, C-weighted [dB] EPNL L5	Plastic ground boards	3, 30 [m]	Fixed-wing Quadcopter Hexacopter	H, F	GPS Weather station Listening experiment
Senzig and Marsan [32]	n.r.	1	1/2" free-field microphone 3 ground mic configurations	PSD	Metal ground boards	150 [m]	Fixed-wing Quadcopter Hexacopter	F	n.r.
Senzig et al. [31]	SPL meter Audio recording system	2	1/2" free-field microphone 1 pole-mounted mic 1 ground plate-mounted mics	SPL, A-weighted [dB] SEL, A-weighted [dB]	Grass Metal ground boards	25, 50, 100, 200 [ft]	Quadcopter	F	Audio recorder. GPS. Weather station
Alexander and Whelchel [36]	Multichannel	5	1/2" free-field microphones: 5 ground plate -mounted mics	SPL, Z-weighted [dB] SEL [dB]	Grass Plywood ground boards	9.14 [m]	Hexacopter	H, F	GPS Weather station
Didkovskyi et al. [37]	Audio recording system	2	1/2" free-field microphone 2 pole-mounted mic	SPL, Z-weighting [dB]	Grass	6.5 [m]	Quadcopter	H, F	n.r.
Cussen et al. [29]	SPL meter	1	1/2" free-field microphones	SPL, A-weighted [dB]	Concrete	5, 10, 30 [m]	Quadcopter	H, F	GPS
Read et al. [33]	SPL meters	3	1/2" free-field microphones: 1 pole-mounted mic 2 ground plate-mounted mics	SPL, A-weighted [dB] SEL, A-weighted [dB]	Mowed Grass Metal ground boards	4, 80, 100,150 [ft]	Quadcopter Hexacopter Octocopter Fixed-wing	H, L, F, iM	Audio recorder GPS Weather station
Besnea [27]	Acoustic camera	64	Underbrink microphone array	SPL Z-weighting [dB] SQM Directivity diagrams	Good ground boards	3 to 61 [m]	Quadcopter Octocopter	H, F, oM	Weather station
Yehorova and Lumnitzer [30]	SPL meters	6	1/2" free-field microphones 6 tripod-elevated mic	SPL, A-weighted [dB]	Grass	1.5, 2, 3 [m]	Quadcopter	F	n.r.
Hui et al. [39]	Spherical microphone array Audio recording system	2	1/2" free-field microphone 1 pole-mounted mic	SPL, A-weighted [dB] SEL [dB] LPN, LTPN SQM and 5-percentiles	Grass	10, 27, 30 [m]	Quadcopter	H, F	GPS Barometer
Beaulieu [38]	Multichannel data acquisition system	4	1/2" free-field microphones 4 tripod-elevated mics	SPL, Z-weighting [dB] SQM	Concrete	0.5, 1.8, 3[m]	Quadcopter	H, F, tM	n.r.
Konzel and Greenwood [41]	Multichannel data acquisition system	14	1/2" free-field microphones 12 ground plate-mounted mics 4 tripod-elevated mics	SPL A, Z-weighting [dB] SEL, A-weighted [dB]	Metal ground boards	50, 100, 200 [ft]	Octocopter	H, T, L, F, oM	GPS Inertial sensors
Cutler-Wood et al. [40]	Multichannel data acquisition system	19	2 ground microphone arrays: linear, circular. 1 elevated array	SPL, Z-weighted [dB] Directivity diagrams	Grass Metal ground boards	50 to 100 [m]	Hexacopter	H, T	GPS Weather station
Wunderli et al. [22]	Multichannel data acquisition system	5	1/2" free-field microphone: 3 ground mic, 2 pole-mounted mic	SPL, Z-weighted [dB] SEL [dB]	Metal ground boards	6 [m]	Quadcopter Hexacopter	F,H	GPS

* sUAS small Unmanned Aerial System, SEL Sound Exposure Level, SPL Sound Pressure Level, EPNL Effective Perceived Noise Level, LPN mean Perceived Noise Level.
LTPN Tone-corrected Perceived Noise level, HOA higher-order Ambisonics, SQM Sound Quality Metrics, GPS Global position system, n.r. not reported.
H Hovering, T Take-off, L Landing, F Flyover, iM inspection manoeuvres, tM transient manoeuvres, oM other manoeuvres.

Table 2
sUAS features.

Model	sUAS ID	Weight [g]	Payload [g]	Diagonal wheelbase [mm]	Flight speed ν [m/s]		Number of rotors N_r	Number of blades N_b	Propeller diameter D [m]
					Fast	Slow			
DJI Matrice 300 RTK	*M3*	6300	930	895	15.0	5.0	4	2	0.53
Yuneec H520E	*Yn*	1633	350	520	13.5	5.0	6	2	0.24
DJI FPV	*Fp*	795	-	245	27.0	15.0	4	3	0.13
DJI Mini 3 pro	*3p*	249	-	247	15.0	5.0	4	2	0.15

(a) Location of the flight test area in Edzell-Scotland.

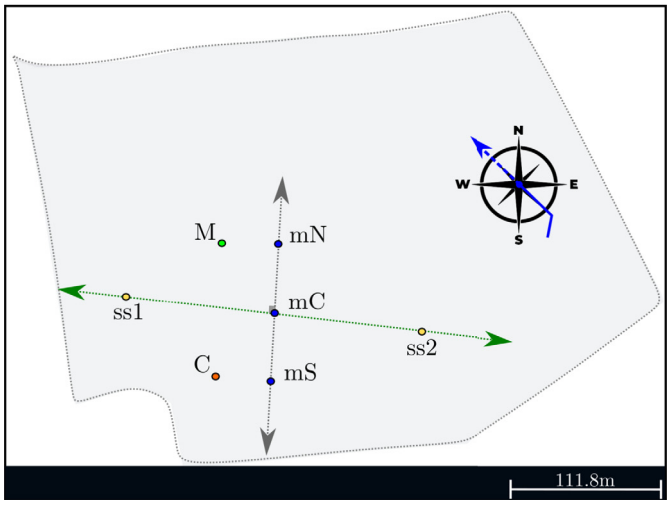

(b) Overview of the flight-path, sensors, and wind direction.

Fig. 2. Geo-referenced location of the farm land used for the drone noise measurements.

3.2. Microphone array

The acoustic measurements were carried out with a ground-mounted microphone setup as proposed by NASA's Technical Group [23]. The horizontal distances for the configuration of nine microphones and the resulting Θ angles with 15° resolution are listed in Table 3 and depicted in Fig. 3b. This microphone array configuration also allows for a subsequent noise hemisphere construction as described in EASA [45].

The microphone setup depicted in Fig. 3a provides a reasonable approximation of a flush mounted configuration over the audible frequency range [46,47]. A small tripod facilitated the installation of a 1/2" free-field microphone diaphragm above the metal plate, as recommended in the noise measurement procedures for propeller-driven aircraft certification in ICAO-Anex 16-Vol 1 [48].

Table 3
Lateral distances required for each microphone position from the centre microphone with $hAGL = 10$ m.

Layout ID Figs. 2 and 4	Mic. Fig. 3b	Distances [m]	Θ [deg]
mN	1	17.32	-60
	2	9.99	-45
	3	5.77	-30
	4	2.67	-15
mC	5	0.00	0
	6	2.67	15
	7	5.77	30
	8	9.99	45
mS	9	17.32	60

Windscreens were used on all microphones. The Data Acquisition System recorded the signal of all microphones simultaneously at a 50 kHz sample rate.

Due to the reflection caused by the presence of the ground plate, sound pressure level were corrected to remove this "doubling effect" in the measured values. This correction is equivalent to reducing the measured sound pressure level by 6 dB across all frequencies [49,47]. It should be noted that this type of setup is limited to reporting results on frequencies below 10 kHz [32]. Fig. 4 presents the complete coordinate system that describes the microphone line array and the transverse flight path.

3.3. Acoustic characterisation

Acoustic metrics

The Sound Exposure Level (L_{AE}) or (SEL) metric represents the sound level, in dBA, of an individual sound event as if that event had occurred within a compressed time, usually one second. Equation (1) evaluates the flyover event by L_{AE} considering the sound level L_p within the time $t'' - t'$, i.e., when L_{Amax} - 10 dB. L_{Amax} is the maximum value of the Overall A-weighted Sound Pressure Level (OASPL) reached during a flyover measurement period expressed in dBA [51,52], where $t_{ref} = 1$ s, and $p_0 = 20$ μPa.

$$L_{Aeq} = 10\log_{10}\left(\frac{1}{t''-t'}\int_{t'}^{t''}\frac{p(t)^2}{p_0^2}\,dt\right)$$
$$L_{AE} = L_{Aeq} + 10\log_{10}\left(\frac{t''-t'}{t_{ref}}\right) \quad (1)$$

Back-propagated sound levels

The back-propagation process aims to calculate the sound levels at a distance r from the source that is closer than the actual position of the microphone, as is depicted in Fig. 3b. In this paper, the back-propagation from the ground microphones to the source at a distance $r = 1$ m was carried out according to ISO 9613-2:1996 [53].

The losses due to spherical spreading σ_∇ [54], atmospheric absorption σ_α [55,56], and the ground plate microphone σ_{ground}

(a) Ground Microphone setup, accordingly to ICAO [50].

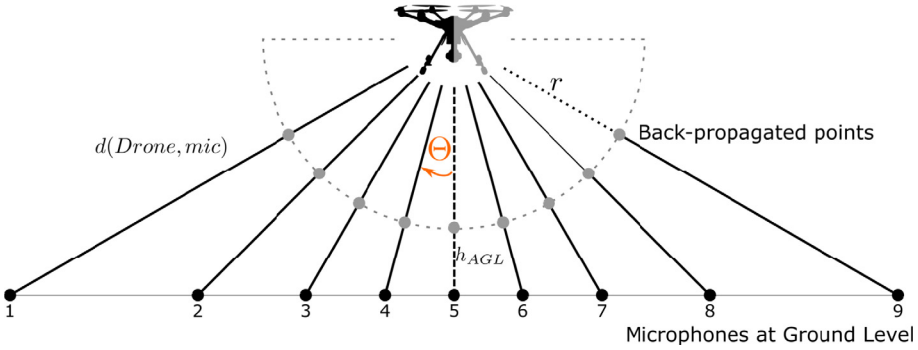

(b) Microphones constant angle resolution and back-propagated points when the sUAS location is just over the microphone array at height h_{AGL}. Figure adapted from [23].

Fig. 3. Ground plate microphone and lateral distances required for each microphone position from the central microphone when $h_{AGL} = 10$ m [23,50].

[49,47] were considered as the main factors influencing the back-propagation of sound signals from ground receiver to source [57]. Equation (2) calculates the required corrections mentioned above between the noise amplitude registered on the ground microphone position $L_{ground}(t)$ and the back-propagated levels $L_{source}(r,t)$ as time-dependent magnitudes [58].

$$L_{ground}(t) = L_{source}(r,t) - \sigma_{\nabla}(t) - \sigma_{\alpha} - \sigma_{\text{ground}} \tag{2}$$

The spherical spreading describes the changes on the sound level as a function of the source-receiver distance. The distance between the source and the receivers $d_{(\text{Drone,mic})}$ is obtained by the Euclidean norm between three points $\in \mathbb{R}^3$ over time, as presented in Equation (3), where $d_x(t)$ is the distance along the x-axis (i.e., flight-path) over time, d_{mic} is the distance in y-axis between the central microphone to each microphone in the array, and h_{AGL} is the aircraft height Above-the-Ground-Level in z-axis, or the aircraft slant range from the central microphone.

$$\left\| d_{(\text{Drone,mic})}(t) \right\| = \left[\Sigma_{(x,y,z)} \text{abs}\left(d_x(t), d_{mic}, h_{AGL}\right)^2 \right]^{1/2} \tag{3}$$

Then, the distance considered for the back-propagated sound levels is the constant radius r with respect to the sUAS centre of mass. Although the value of $r = 1$ m has been suggested [23], values $r > 1$ m could be considered to avoid calculation errors in the near field [54]. Hence, the contribution of the spherical spreading σ_{∇} in dB is derived in Equation (4).

$$\sigma_{\nabla} = 20 \log_{10} \left(\frac{r}{d_{(\text{Drone,mic})}} \right) \tag{4}$$

The losses due to the atmospheric absorption σ_{α} are described by atmospheric sound attenuation coefficient α in Np/m. Air absorption depends on environmental conditions such as humidity, temperature and pressure, together with the frequency of the signal f in Hz.

Equation (5) presents the calculation of coefficient α as a function of the relaxation frequencies for oxygen $f_{r,O}$, and nitrogen $f_{r,N}$, where $p_0 = 1$ atm, and $T_0 = 293.15$ K [59,57].

$$\alpha = f^2 \left\{ \left[\frac{1.84 \times 10^{-11}}{\left(\frac{T_0}{T}\right)^{1/2} \frac{p_s}{p_0}} \right] + \left(\frac{T_0}{T}\right)^{2.5} \left[\frac{0.10680 e^{-3352/T} f_{r,N}}{f^2 + f_{r,N}^2} + \frac{0.01278 e^{-2239.1/T} f_{r,O}}{f^2 + f_{r,O}^2} \right] \right\} \tag{5}$$

Thus, the attenuation of sound pressure levels due to atmospheric absorption in dB is obtained by Equation (6) [55,60].

$$\sigma_{\alpha} = 10 \log_{10} e^{2\alpha r} \tag{6}$$

Finally, corrections were made in the measured sound pressure levels due to the reflective ground plate setup (see Fig. 3a). The influence of the ground plate reflection becomes well defined at frequencies below 10 kHz [47,49]. Then, the doubling of pressure corresponds to a 6 dB increase from the free-field condition.

$$\sigma_{\text{ground}} = 6 \tag{7}$$

As the microphones were placed on ground plates, ground effects in the form of constructive and destructive interference between direct and reflected sound waves were not considered.

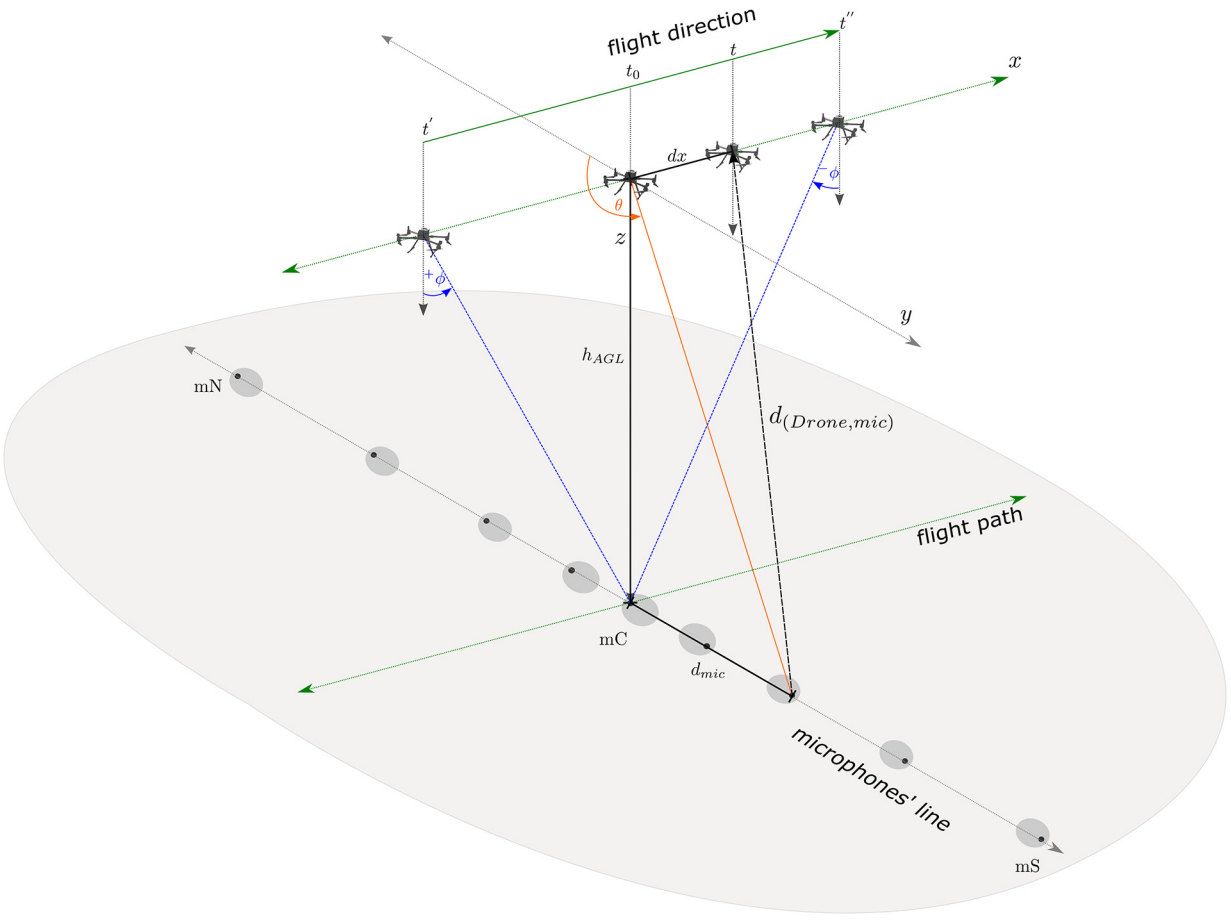

Fig. 4. Coordinate system for noise measurements during flyovers.

Directivity

The construction of noise hemispheres for conventional rotorcraft has been well defined and provides an adequate technique to present the complex nature of the sUAS directivity from measured acoustic emissions during dynamic flyovers and static tests [19,45,40,61].

The directivity is derived by the back-propagated sound levels recorded at ground positions (see Fig. 5a) and the collection of discrete noise sources across different noise source locations (see Fig. 5b) [19].

From a practical point of view, if GPS tracking data is not available or the data-time resolution is not enough compared to the sUAS flight speed, the sUAS position over time could be derived from an estimated position of reference. Then, the sUAS position could be determined each time as $d_x(t)$. In this case, these reasonable assumptions are taken into account: *(i)* The sUAS speed and h_{AGL} are constant during the flyover test: *(ii)* The sUAS flight path is transversal to the microphone's array over the central microphone; *(iii)* The maximum level of noise emission is recorded when the sUAS crosses the microphone line.

The noise data at each source position $d_x(t)$ could then be estimated from the time before and after $d_x(t_0)$ (see Fig. 4). Finally, the back-propagated levels can be calculated on the matrix conformed by the horizontal angles Θ from the microphone position and the polar angles ϕ from the sUAS flight path, as depicted in Fig. 5c. Based on this approach, the back-propagated sound levels at radius r allow the construction of both the 2D horizontal directivity $L(0°, \Theta, r)$ when L_{Amax} is recorded, and the 3D noise hemispheres $L(\phi, \Theta, r)$ from compact noise sources distributed over time t' to t''.

3.4. BPFs and rotors performance

Fuerkaiti et al. [62] reported effects on the single propeller noise footprint due to the variations in the Advance Ratio J (Equation (8)). The effects are *(i)* changes in the noise directivity and the amplitude of the harmonics of the Blade Passing Frequency (BPF), and *(ii)* the reduction in the on-ground noise levels when J increases.

$$J = \frac{v[\text{m/s}]}{RPS \cdot D[\text{m}]} \tag{8}$$

The parameter J has also been reported for multirotor systems when all propellers rotate at the same speed [63]. Since the differences in the rotational speed of the propellers determine the velocity of the sUAS relative to the ground [64], this study uses an averaged Advance Ratio as $\overline{J}$ for aerodynamic scaling of the acoustic metrics and directivity.

The rotational speed of the individual sUAS rotor is derived from the $n \in N_r$ peaks identified as the local maximum in the low-frequency range of the acoustic spectrum, as presented in Fig. 6, where f_0 is the averaged BPF.

4. Results

The weather conditions reported during the measurement campaign at 10 m height include the Relative Humidity in H%, Air Temperature in °C, Wind Speed in m/s, and Barometric Pressure in mbar. Throughout the measurement period, the air temperature ranged from 13 to 16 °C (55 to 61 °F) with average wind speeds generally between 0 to 6 m/s and a prevailing wind direction from

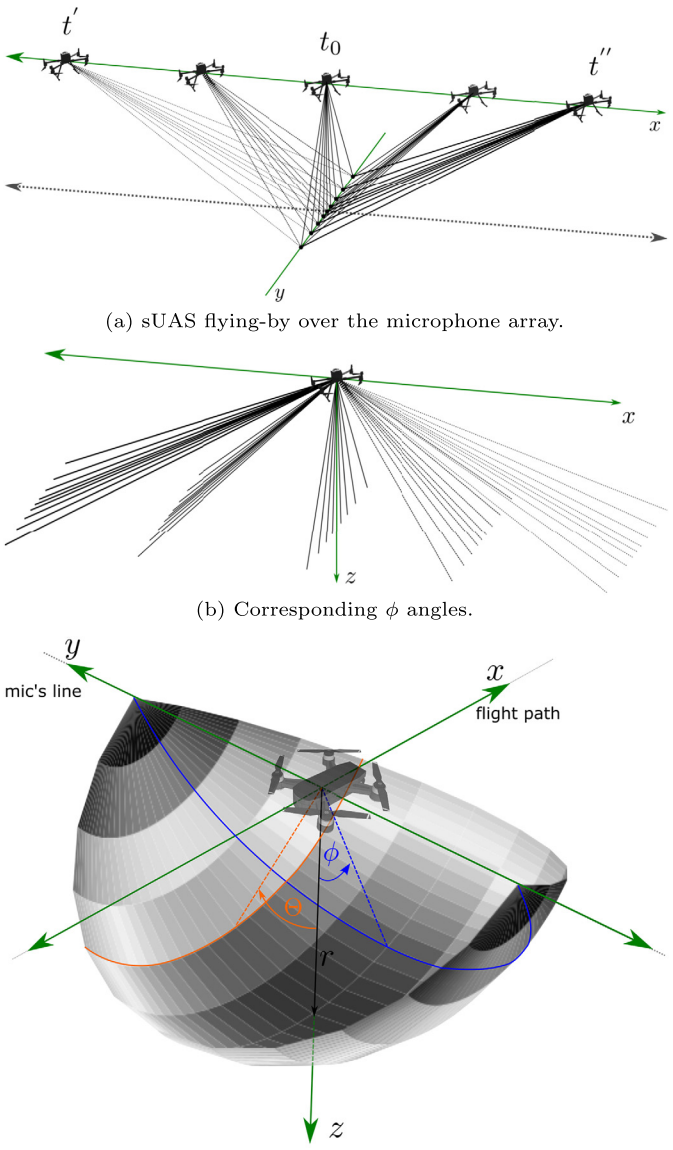

(a) sUAS flying-by over the microphone array.

(b) Corresponding ϕ angles.

(c) Resulting sUAS Noise Hemispheres.

Fig. 5. sUAS Noise Hemispheres construction. Adapted from Hobbs et al. [19].

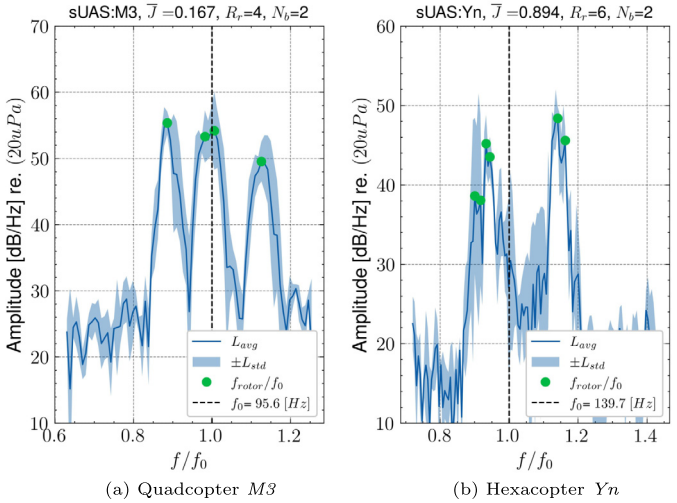

(a) Quadcopter *M3*

(b) Hexacopter *Yn*

Fig. 6. BPF peaks relative to f_0 during flyovers for (a) 4-rotors sUAS at M = 0.044, and (b) 6-rotors sUAS at M = 0.039.

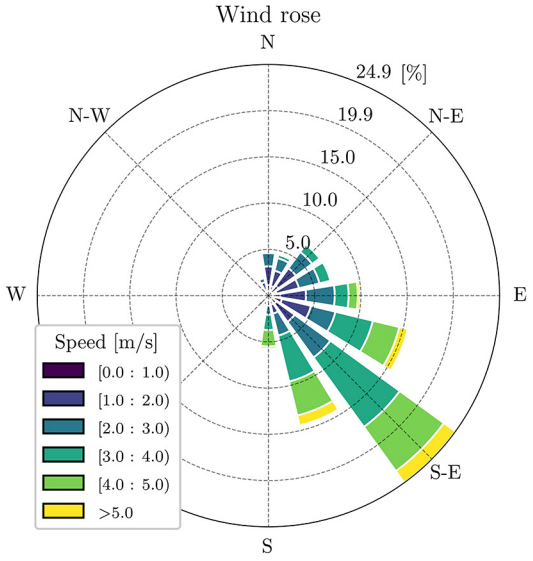

Fig. 7. Representation of wind speed in m/s and direction for 17th of August 2022, from 12:00 to 17:00. Wind from the southeast quadrant almost 60% of the time.

the southeast. Special attention was paid to both wind speed and direction as the interaction of wind flows with aircraft and rotating elements of sUAS has been found to highly influence sUAS noise emission [25,43,41].

Fig. 7 shows that most of the wind speed readings registered by the sonic anemometer remained lower than the minimum sUAS speed tested i.e., 5 m /s in the fairly stable southeast to northwest wind direction. Based on the direction of the wind, and the position of the flight start/stop points depicted in Fig. 2, it is possible to define the flyover operation as “downwind” when the sUAS flies from east to west and “upwind” when west to east.

Acoustic metrics

The average ambient noise level (35 dB L_{Aeq}) was low enough to allow the recording of the acoustic signal of the sUAS. More than 10 dB signal-to-noise ratio (i.e., measured sound pressure levels over background noise) was possible in all microphone positions, meeting the 3 dB recommended by NASA-UNWG-Subgroup 2 [23].

The comparison of the L_p time histories relative to $t_{L_{Amax}}$ of different sUAS and flight conditions at central-microphone is presented in Fig. 8.

Fig. 8a shows four different flyover conditions for the sUAS *M3* at two Mach number (M), and two TOW. The higher the flyover speed, the higher L_{Amax} and the shorter the exposure time. At same M, the slight reduction in L_p when increasing $\overline{J}$ agrees with the acoustic data reported in the literature for a single propeller [62]. The influence of $\overline{J}$ on L_p seems to be higher for the cases with lower M.

Fig. 8b shows four different sUAS flyovers at high speed (see Table 2). Among the quadcopters, the largest and heaviest one *M3* produced the highest L_p. *M3* has the lower $\overline{J}$ from all the sUAS tested. Despite the significant difference in TOW, the hexacopter *Yn* generates similar L_p as the quadcopter *Fp*. The differences in flyover speed and blade count (and also number of rotors) between the *Yn* and *Fp* sUAS are reflected in the $\overline{J}$. The higher $\overline{J}$ of the *Yn* seems to compensate the higher TOW for noise emission (as compared to *Fp*). Important differences in the rear arc of the polar Θ directivity are observed between the different sUAS tested.

The effect of sUAS TOW on the reported L_{AE} has also been investigated. The very-strong positive Pearson correlation between L_{AE} and TOW at constant flyover speed is presented in Fig. 9. General analysis of the correlation supports the hypothesis that sUAS

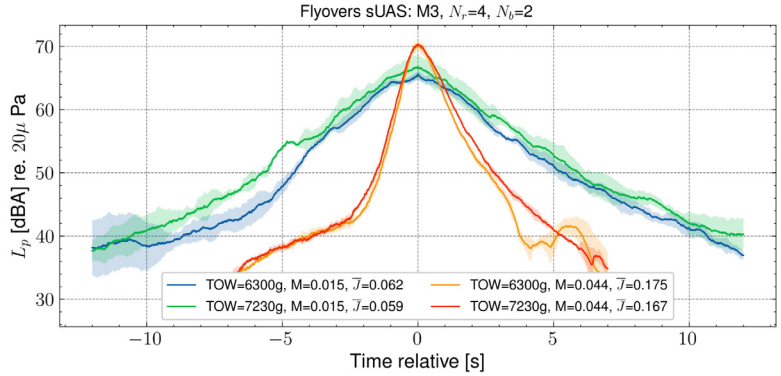

(a) A-weighted sound pressure level vs. time curves of four flyover conditions of sUAS *M3*.

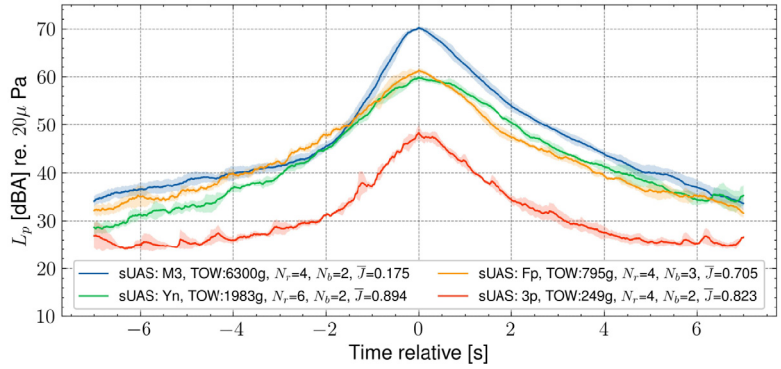

(b) A-weighted sound pressure level vs. time curves of fast flyover of sUAS *M3, Yn, Fp* and *3p*.

Fig. 8. A-weighted sound pressure level vs. time curves reported from central-microphone during flyovers. Standard deviations from averaging three consecutive downwind flyover events are included.

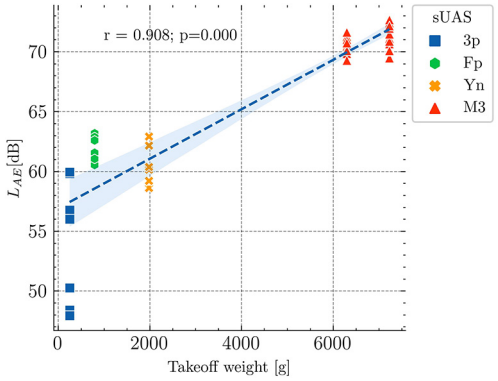

Fig. 9. Coefficient of linear correlation for L_{AE} and sUAS Takeoff weight (TOW). The Sound signal at the central microphone. Two groups of data are presented for the drone *M3*, without and with the payload attached.

are noisier the higher their payload or the faster they fly (see Fig. 8a).

In general, all sUAS spectrograms show a very clear propeller-related noise at deterministic low-frequency narrow band and prominent tonal components at harmonics (see Fig. 10), as is described by Wu et al. [13]. During controlled and stable operations (e.g. hovering operation in laboratory conditions), the noise frequency spectra might show very clear tonal components related to the BPFs and shaft frequencies. This is not always the case for other more complex operations, such as flyovers in real scenarios [36].

The BPFs narrow-band and upper harmonics of the bow and stern rotors are illustrated in the spectrograms in Fig. 10 where the frequency axis is normalised by the average Blade Passing Frequency (BPF) f_0. Due to the forward flyover operation, the bow propellers have slightly higher RPM than the stern propellers.

Moreover, the larger the size of the sUAS (airframe and/or propellers), the larger the broadband component; this effect is due to, among other noise generation mechanisms, due to the unsteady pressure fluctuations caused by turbulence and boundary layer interactions with the edges of the blade [43].

The Doppler effect is also captured in the spectrograms as a common characteristic of the moving sources from the fixed position receiver (i.e., Eulerian specification). These frequency shifts could be included for an accurate representation of acoustic signals, such as the separation of both specific tonal and broadband component, or on the noise source analysis when the receiver is attached to the moving source [65] (i.e., Lagrangian specification). The results presented in this paper have not been corrected to remove the Doppler effect. The main reasons are that the sUAS were measured at very low M, leading to a very reduced Doppler shift (see Fig. 10); and the tonal noise analysis was done in a frequency band basis, with these bands defined to include the specific tonal noise of interest, including the frequency shift due to the Doppler effect. De-Dopplerised acoustic signals would be needed if an auralisation process is intended. For further details, see Section 5.

Back-propagated levels

Once the back-propagated metrics are obtained, it is feasible to present directivity plots by OASPL or by a representation of frequency bands, such as 1/3 octave bands. In particular, this section presents the results of L_{Amax} back-propagated over the microphone line, and OASPL of a time-segmented signal in a 3D model, as currently applied for conventional aircraft certification [45,19].

2D directivity based on L_{Amax} event

The noise directivity patterns were calculated on the assumption that L_{Amax} is measured at the point where the sUAS is in the

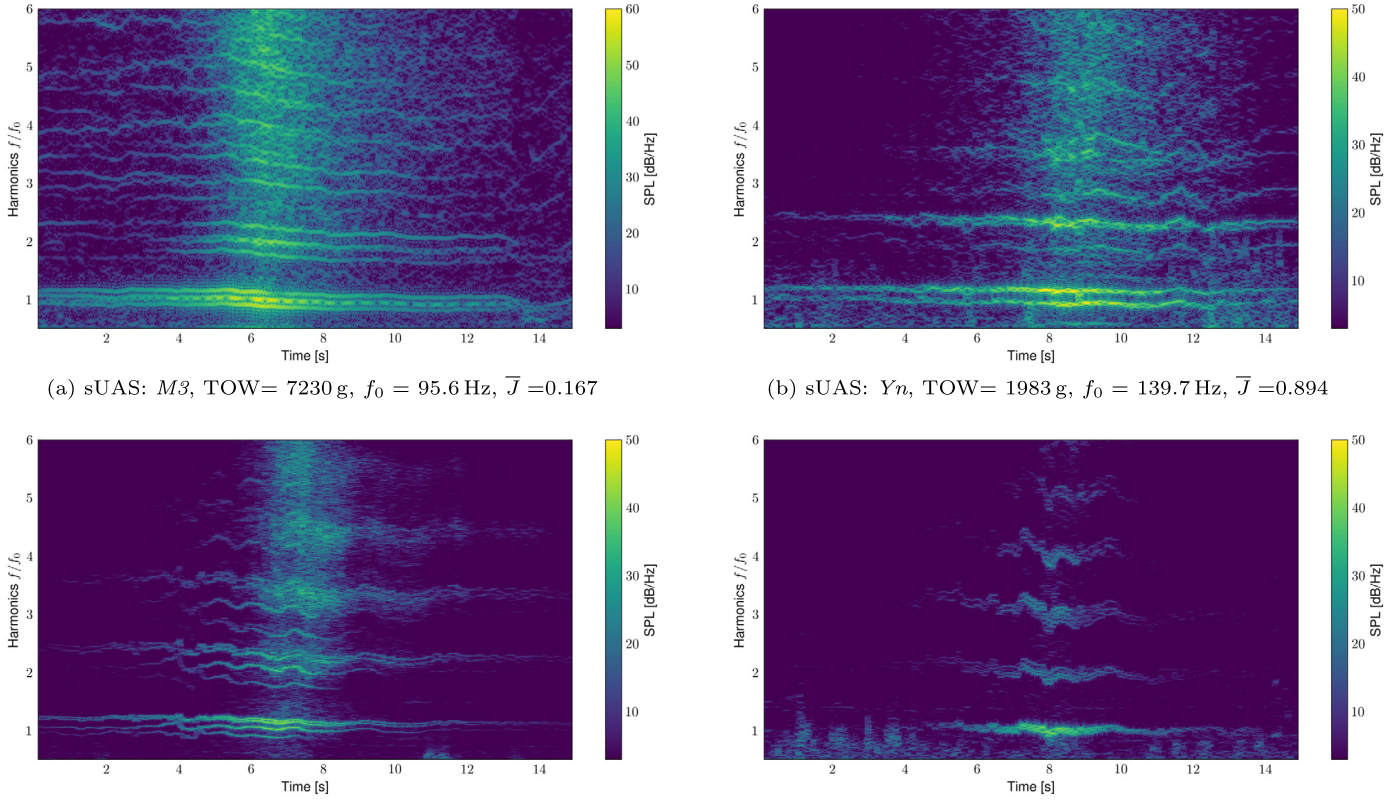

(a) sUAS: *M3*, TOW= 7230 g, f_0 = 95.6 Hz, $\overline{J}$ =0.167

(b) sUAS: *Yn*, TOW= 1983 g, f_0 = 139.7 Hz, $\overline{J}$ =0.894

(c) sUAS: *Fp*, TOW= 795 g, f_0 = 474.2 Hz, $\overline{J}$ =0.705

(d) sUAS: *3p*, TOW= 249 g, f_0 = 243.0 Hz, $\overline{J}$ =0.823

Fig. 10. Spectrograms at central microphone position during high speed sUAS downwind-flyovers and h_{AGL} = 10 m.

closest proximity to the microphone line. This approach enabled the plotting of the back-propagated maximum level at Θ angle ($-60° \leq \Theta \leq 60°$) at $\phi = 0°$. The directivity of the OASPL, the corresponding 1/3 octave of the BPF, the BPF's first harmonic, and the broadband noise component are plotted in Fig. 11. The process of decomposing the signal into tonal and broadband components can be accomplished by applying a moving-median filter to the spectra of each individual microphone [66].

In general, all sUAS directivity patterns are presented symmetrically from $\Theta = 0°$, with differences less than 2.5 dB for symmetric horizontal angles. In the sUAS *M3* and *Yn*, with higher TOW, there is a difference of less than 3 dB between the OASPL and the broadband noise component, suggesting the dominance of broadband over tonal noise. For the smaller sUAS, i.e., *3p* and *Fp*, the relative contribution of tonal noise to the OASPL is higher, especially in the case of the *3p* sUAS. The amplitude of the BPF and BPF's first harmonic is different for each type of sUAS tested. The relative contribution of tonal vs. broadband noise can also be seen in the spectrograms shown in Fig. 10.

Fig. 12 presents the directivity of the correspondent 1/3 octave bands of f_0, two first BPF harmonics, the broadband noise component and OASP for four different flyover conditions tested for the sUAS *M3*, i.e., at two different M and two different TOW. As observed in Fig. 12, the directivity of the OASPL and broadband noise component are similar for all the cases tested; the amplitude of both OASPL and broadband noise increases with both TOW and M. Tonal noise also increases with M. At M = 0.015, a decrease in $\overline{J}$ let to a small increase in the amplitude of the 2nd BPF harmonic; at M = 0.044, a decrease in $\overline{J}$ let to a small increase in the amplitude of the 1st BPF harmonic. The directivity pattern for the different tonal components is more complex, likely due to the unsteady noise signature usually found in sUAS, and potential shielding effects. Even with a small decrease in $\overline{J}$, tonal noise increases in amplitude. This is consistent with the findings presented by Fuerkaiti et al. [62].

3D directivity based on L_{AE} time

Hemispheric directivity was derived from the flyover data recorded with the microphone array on the ground. The time frame was selected to include the period where the sound level is within the range of L_{Amax} - 10 dB, i.e., $t'_{L_{Amax}-10} \leq t \leq t''_{L_{Amax}-10}$.

As an example, Fig. 13 presents the OASPL noise hemisphere for the sUAS *M3* derived from back-propagated sound levels considering the coverage angles $\phi : (-\phi_{t'} \leq \phi \leq \phi_{t''})$ and $\Theta : (-60° \leq \Theta \leq 60°)$. The same procedure can be applied to show results using other calculated acoustic metrics available in the time domain after back-propagation, such as sound level per octave or 1/3 octave bands.

A plain representation of the noise hemispheres is depicted in Fig. 14. Symmetrical directivity over the horizontal angle Θ presented in Fig. 11 is also depicted in this unwrapped noise hemispheres. However, information carried out in the flyover time domain improves the description of noise directivity over polar angles ϕ.

As shown in Fig. 14, the maximum noise radiation for the four sUAS tested is contained in the rear arc of the polar directivity. The larger sUAS show a well define 3D directivity, while the 3D directivity of the smaller sUAS is more complex. This is likely due to the unstability of these smaller sUAS during the flyover tested. The ϕ angles of maximum radiation are between 20° and 20° for all the quadcopter, and between 40° and 60° for the hexacopter *Yn*. Although presenting more complex patterns, these results are in line with some previous studies finding maximum noise radiation of single propeller noise at the rear arc of polar angles [62].

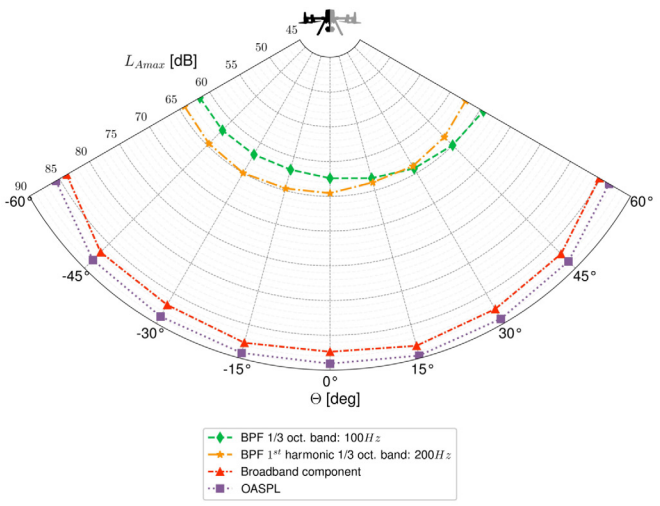

(a) sUAS: *M3*, TOW= 7230 g, f_0 = 95.6 Hz, $\overline{J}$ =0.167

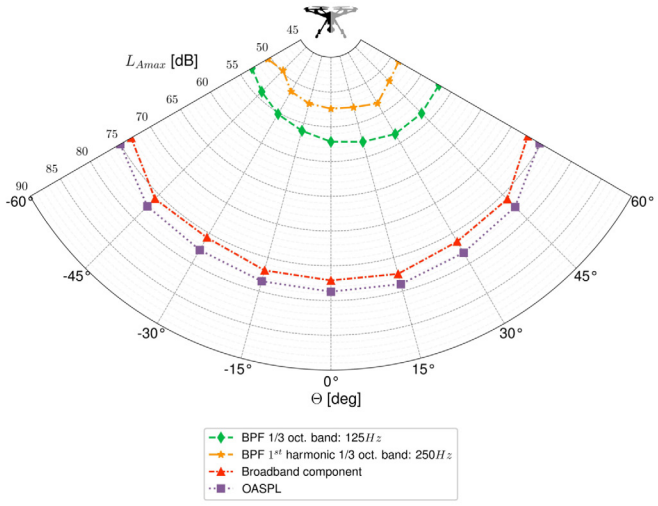

(b) sUAS: *Yn*, TOW= 1983 g, f_0 = 139.7 Hz, $\overline{J}$ =0.894

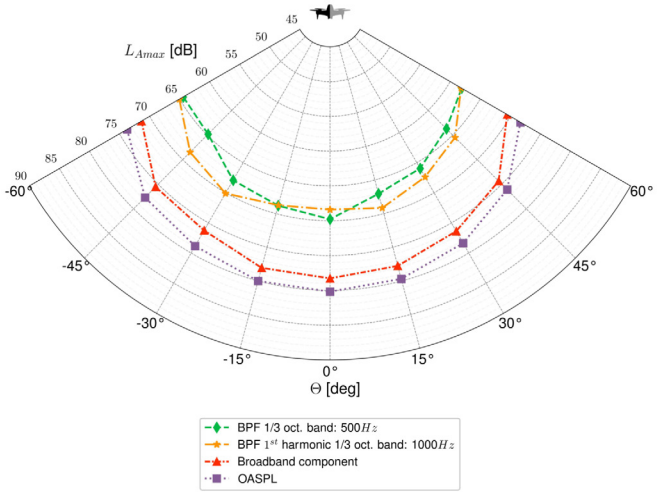

(c) sUAS: *Fp*, TOW= 795 g, f_0 = 474.2 Hz, $\overline{J}$ =0.705

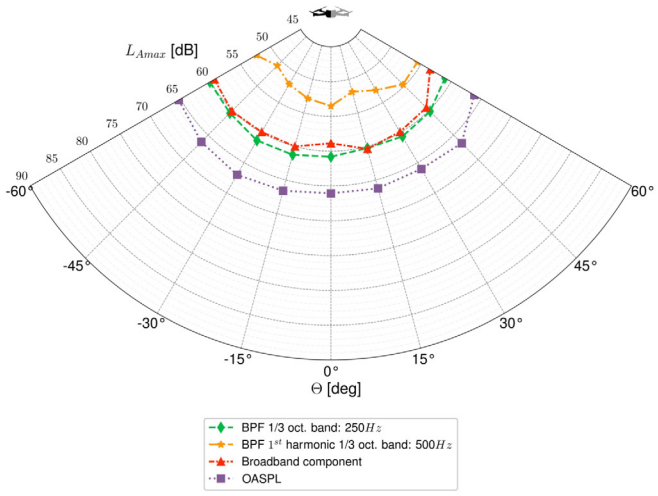

(d) sUAS: *3p*, TOW= 249 g, f_0 = 243.0 Hz, $\overline{J}$ =0.823

Fig. 11. Noise directivity for high speed sUAS downwind-flyover at h_{AGL} = 10 m.

5. Discussion

Noise measurements

The selection of the microphone array configuration and measurement procedure used in the acoustic characterisation described in this paper was based on the guidelines provided by technical working groups [23,24]. These emerging guidance documents served as a valuable reference to ensure that the presented methodology adhered to standards and best practices in the field.

Recently, the European Union Aviation Safety Agency (EASA) has published its guidelines on noise measurement of UAS lighter than 600 kg operating in the specific category [42]. These guidelines recommend a measurement protocol for both flyover and hover operations, requiring only a single ground plate microphone directly underneath the flight path. The methodology described in these EASA guidelines is generally more simplistic than the methodologies presented within either the ISO [24] or UNWG [23] documents and is more closely aligned to the one described by ICAO [48].

One limitation of the approach recommended by EASA is that does not allow the development of noise hemispheres including directivity data, which could be highly valuable for environmental noise modelling [42] and auralisation [67]. Another interesting observation about EASA guidelines is that the noise emission from the flight procedures is recommended to be defined using L_{AE} and L_{Aeq} for the flyover and hover operations respectively. However, the guidelines do not include recommendations about noise criterion for L_{Amax}. This is likely a result of a current lack of evidence to justify these criteria.

Existing guidance stresses the importance of accurate positioning data and that it needs to be recorded as part of a noise measurement campaign [23,24]. To meet these requirements, the recommendation is generally to measure sUAS spatial positioning and speed using Augmented Global Navigation Satellite Systems (GNSS). However, the measurement and analysis procedure presented in this paper allows for reduced variability in the acoustic result of the different sUAS measured under actual operations outdoors without the use of a GNSS. Since approximately half of the flights were made in one direction of travel and half in the other, any systematic failure would have resulted in a lack of consistency of the measurements taken in the first direction compared to those taken in the second. Although it is possible that the effect of the sUAS or microphone location could have influenced the results, it was found to be non-deterministic, as no significant differences

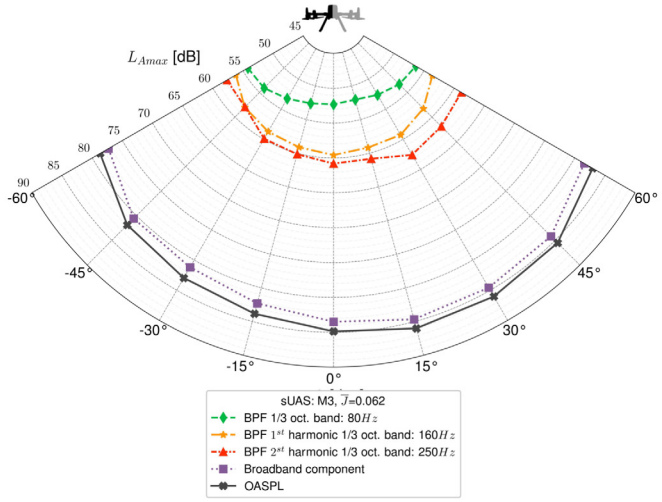

(a) TOW=6300 g, M=0.015, f_0 =58.6 Hz, $\overline{J}$=0.062

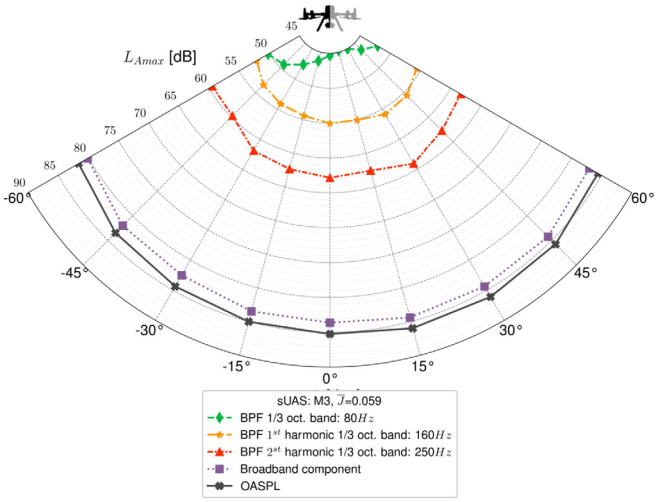

(b) TOW=7230 g, M=0.015, f_0 =90.4 Hz, $\overline{J}$=0.059

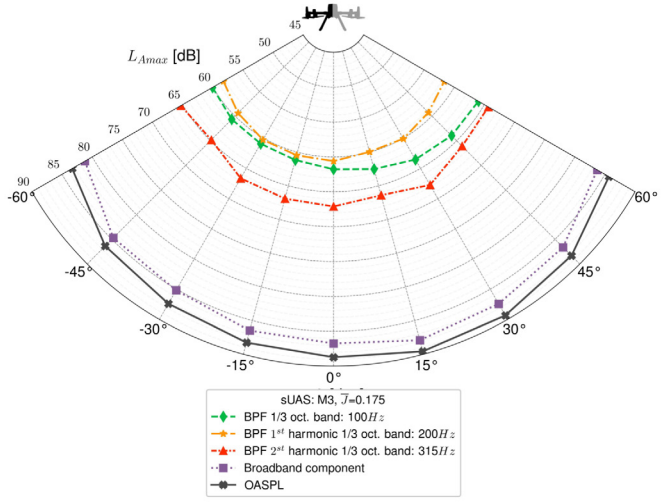

(c) TOW=6300 g, M=0.044, f_0 =91.6 Hz, $\overline{J}$=0.175

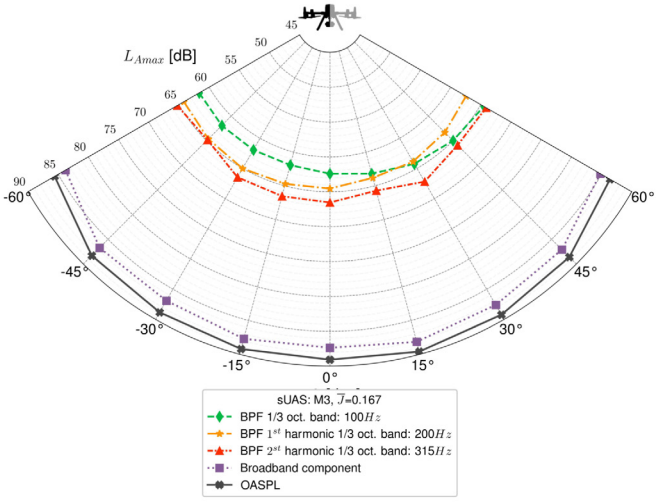

(d) TOW=7230 g, M=0.044, f_0 =95.6 Hz, $\overline{J}$=0.167

Fig. 12. Noise directivity of four different flyover conditions of sUAS *M3* at h_{AGL} = 10 m.

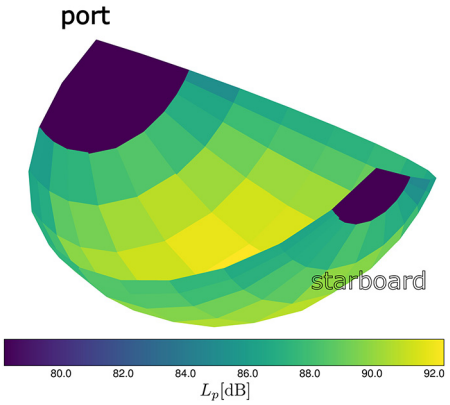

Fig. 13. 3D representation of the constructed OASLP noise hemispheres for downwind flyover of sUAS *M3*.

were observed between the two flyover directions, resulting in moderate variability of the results. In fact, the results suggest that the navigation systems themselves provide sufficient accuracy and precision to meet the flight procedures required under the measurement protocol, and therefore the theoretical calculations based on nominal data are sufficiently reliable for sUAS characterisation even if sUAS detailed positioning data tracking is not available during processing. However, an in-depth study of the uncertainties due to the lack of GNSS data for the acoustic data measured should be determined in further work.

Acoustic metrics

As pointed out above, L_{Aeq} and L_{AE} are the metrics recommended for hover and flyover operations respectively [42]. However, no consensus has yet been reached on what metrics should be used to assess the community noise impact due to sUAS operations. Should an event-based criteria be assumed, it could be based upon the number of exceedances over an L_{Amax} criterion during a period of time (e.g., 23:00 – 07:00 hours during night time to avoid sleep disturbance). Also, should criteria requiring noise to be averaged over a period of time be adopted, such as $L_{Aeq,8hr}$, then the L_{AE} associated with each event would be the key noise metric for event characterisation.

As discussed by Torija and Clark [1], assuming sequences of sUAS events emerging from existing background, a more "eventful" scenario might take place. In that case, such "eventfulness"

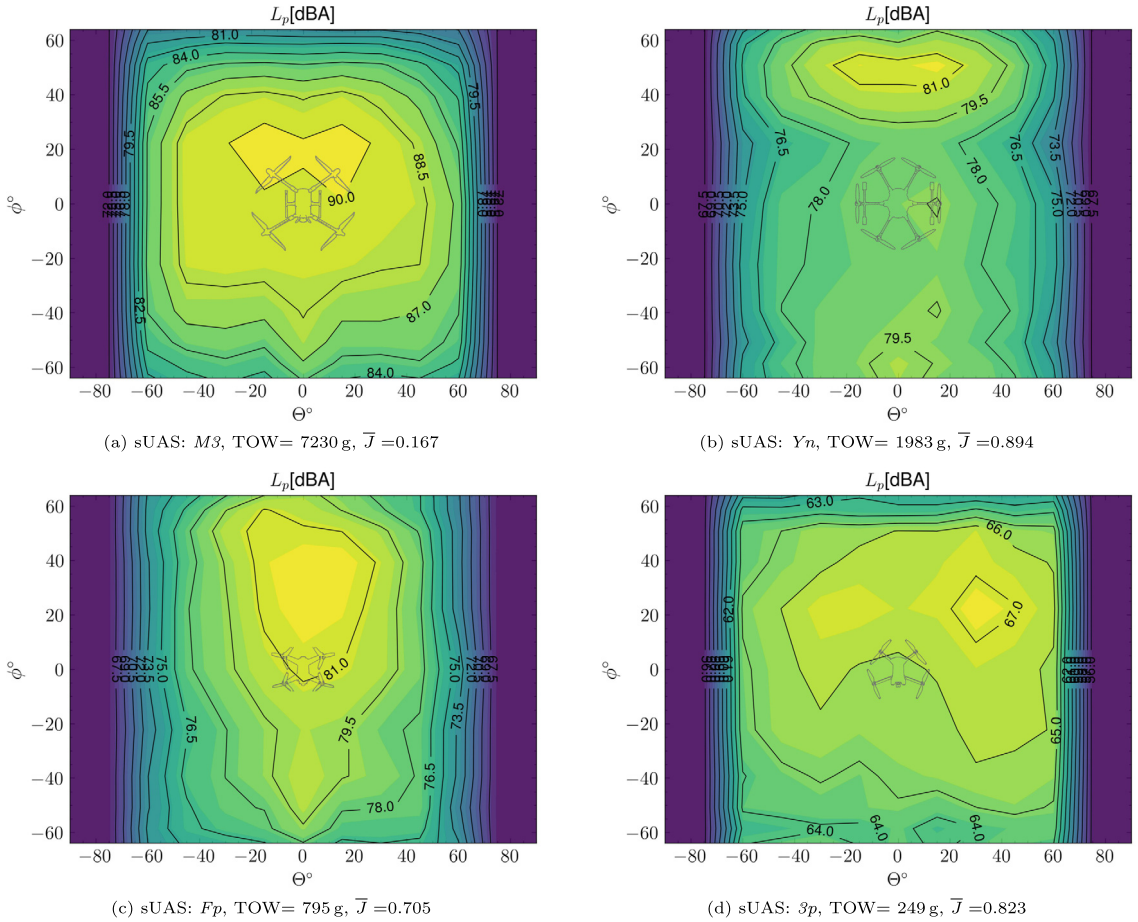

(a) sUAS: *M3*, TOW= 7230 g, $\overline{J}$ =0.167

(b) sUAS: *Yn*, TOW= 1983 g, $\overline{J}$ =0.894

(c) sUAS: *Fp*, TOW= 795 g, $\overline{J}$ =0.705

(d) sUAS: *3p*, TOW= 249 g, $\overline{J}$ =0.823

Fig. 14. Unwrapped representation of the constructed OASLP noise hemispheres for high speed sUAS downwind-flyover at h_{AGL} = 10 m. Flight direction from positive to negative ϕ. sUAS images are presented for position reference.

could be described using metrics such as the Intermittency Ratio (IR) [68] and Noise and Number Index (NNI) [69].

For conciseness, this paper presents L_{Amax} results from the measurements and further calculations of L_{AE}. In addition, the emissions characterisation might also be presented according to ISO 9613-2:1996 [53], using sound power level (L_W) and directivity index (DI), which would be helpful in environmental noise simulations (e.g. in strategic noise mapping) [70].

A more in-depth frequency analysis can be also carried out with the method presented in this paper, to investigate changes in BPF harmonics with operating conditions, and therefore assess contribution of loading and thickness noise [43,41,71,72].

Back-propagation

Back-propagation methods were implemented to characterise the noise directivity of the sUAS measured. As the main sound propagation effects described in ISO 9613-2 have been included in the derivation, the applied method makes the acoustic description of sUAS possible independently of the environment in which the data were obtained. This paper uses a derivation of the polar angle ϕ during the flyover as no GPS-tracking data was available. Therefore, the covered angle ϕ is estimated from the reasonable practical assumption that the L_{Amax} of the sUAS flyover happens at the slant distance ($\phi = 0°$). However, if GPS-tracking data were available from high resolution tracking systems (e.g. GNSS), the derivation of the sound levels over the polar angle ϕ could be more accurate. These GNSS are usually attached on the aircraft and allow a synchronisation with the acoustic acquisition system as is described by Read et al. [33], and Mobley and Campbell [61].

In this paper, de-Dopplerisation was not carried out during the back-propagation as the focus was on propagating back the sound levels to an arbitrary distance from the source. Indeed, the maximum shifting due to the Doppler effect during sUAS flyovers is ±0.3 one-third-octave bands, and is assumed not significant enough to require a de-Dopplerisation, as reported by Mobley et al. [58]. However, if the focus is to back-propagate the broadband and tonal components for auralisation purposes, such de-Dopplerisation is essential, and as such will be considered for further refinements of the presented procedure. Fig. 15 shows the spectrogram for the sUAS *M3* with and without the frequency shift due to the Doppler effect. The de-Dopplerisation algorithm implemented was developed by Greenwood and Schmitz [73].

sUAS noise mapping

The simulation of sUAS operations and their associated noise emission is key for the appropriate management of this new source of environmental noise, as discussed by Bian et al. [74]. The acoustic characterisation provided in this paper, with information about sound levels, frequency content and directivity could be used for the preparation of strategic noise maps for sUAS operations.

In addition, simulation tools can also be used to determine the noise impact incurred by each operation, or the cumulative noise footprint of a service provider, thus enabling new possibilities for the management of sUAS noise. To do that, an appropriate characterisation of sUAS under real operations and representative operating conditions is needed. Furthermore, simulations could be extended for producing dynamic noise maps, as real-time estimation of sound levels at a grid of receivers on the ground to aid decision making for community noise impact.

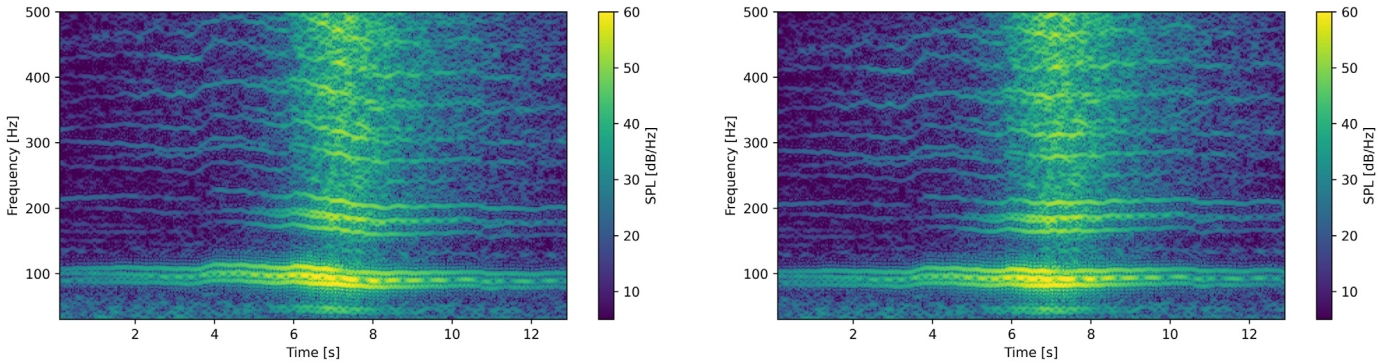

(a) Flyover signal with natural Doppler effect.

(b) Flyover signal including de-Dopplerization.

Fig. 15. sUAS: *M3*, TOW = 7230 g, $f_0 = 95.6$ Hz, $\overline{J} = 0.167$ at M = 0.044.

Table 4
Sound Quality Metrics description.

SQM	Units	Brief description [75,76]	Standard/Model
Loudness N	sone	The sensation value of the human perception of sound volume.	DIN45631/A1
Sharpness S	acum	The sensation value due to high-frequency components.	DIN45692
Fluctuation Strength F	vacil	The very-low frequency variation of the signal amplitude or frequency.	Hearing Model
Roughness R	asper	The low-frequency variation of the signal amplitude or frequency, resulting in an impression of pulsation or beat.	Hearing Model
Tonality T	tuAT	The signal content of individual tones or narrow-band noise.	Aures/Terhardt

Sound Quality Metrics

Linear representation of physical quantities of sound based on human auditory perception is feasible in the psychoacoustic domain by means of the Sound Quality Metrics (SQM) listed in Table 4 [75,76].

SQMs have been investigated as key factors in the prediction of noise annoyance for both conventional rotorcraft [77,78] and sUAS [79]. Gwak et al. [21] suggested the concentration of acoustic energy in the high frequency region is one of the main differences between the noise signature of the sUAS and conventional civil aircraft. Noise annoyance associated with sUAS operations has been found to be primarily influenced by Loudness, Sharpness (i.e., high frequency content) and Fluctuation Strength (i.e., amplitude modulation due to interaction between rotors [79].

Read et al. [80] also suggested that metrics optimised for sUAS noise should include a finer resolution in both time and frequency (compared to traditional aircraft noise metrics) due to the frequency and temporal characteristics of sUAS noise. It is therefore recommended that an analysis of sUAS noise includes SQMs. Fig. 16 shows the 5^{th} percentile for four sUAS (Drones) flying over the microphone line array at 15 m/s, 10 m h_{AGL}.

The Loudness metric (Fig. 16a) is closely related to the physical sound intensity in the receiver position. Therefore, it correlates with the amplitude of noise emitted from each sUAS, reported in Fig. 8. Also, that is the reason why the amplitude is higher at the central microphone and decreases at the wider microphone positions that are at a greater distance, as demonstrated within the measurement campaign. This might be due to the characteristic directivity pattern of most multi-copters with higher sound radiation downward compared to the side, as discussed by [22,65,81].

The presence of high-frequency noise produces a sensation of sharpness [82]. The values of Sharpness per microphone and type of sUAS are presented in Fig. 16b. The dominant spectral content at mid-low frequencies and the lower amplitude of broadband noise at higher frequencies might be the reason for the lowest values of Sharpness for the sUAS *3p* (see Fig. 10). As the value of Sharpness increases by a factor of 50 from 200 Hz to high frequencies near 10 kHz [82], *Fp* demonstrates higher values primarily because of that the most of its sound energy is concentrated from frequencies starting at 400 Hz.

The values of Fluctuation Strength (i.e., slow amplitude modulation of the sound level) per microphone and type of sUAS are presented in Fig. 16c. In the sUAS *Yn*, *Fp* and *3p* the minimum value of Fluctuation Strength is found at microphone M5, while the values of this SQM increase with azimuthal Θ angles. For instance, the sUAS *Yn* has significantly higher values of Fluctuation Strength at microphones M3 and M7. These correspond to Θ angles $\pm 30°$, and are consistent with the angles of maximum emission of amplitude modulated sound in small-scale rotor noise found by Baars et al. [83]. The sUAS *M3* presents the lowest values of Fluctuation Strength. This might be due to the higher distance between rotors in this sUAS, leading to less interaction between rotors (see Torija et al. [84]).

The value of Roughness, as shown in Fig. 16d, is significantly higher for the *M3* sUAS, compared to the other sUAS tested. In principle, this was unexpected, as this sUAS is the largest one tested, and therefore the more stable during flyover. However, as seen in Fig. 10, this sUAS has the highest content of broadband noise in the mid-to-high frequency region. A high content in broadband noise at this region has been found to lead to higher values of roughness for rotor noise [85].

Finally, the Tonality metric in Fig. 16d confirms the effects shown above in the spectrograms in Fig. 10, where the smaller sUAS *3p* and *Fp* have the largest differences between the broadband and the tonal noise; whereas, the sUAS *M3* and *Yn* have broadband and tonal noise of similar magnitude.

6. Conclusions

This paper presents a method for the acoustic characterisation of sUAS under real operations. Based on a robust procedure for the dynamic noise emission characterisation of rotorcraft, and state-of-the-art methods for receiver-to-source backpropagation, the presented method allows a comprehensive characterisation of the noise emission of sUAS, including sound level, frequency spectra and directivity information. The method is flexible as it allows the calculation of several time-varying noise metrics, and detailed fre-

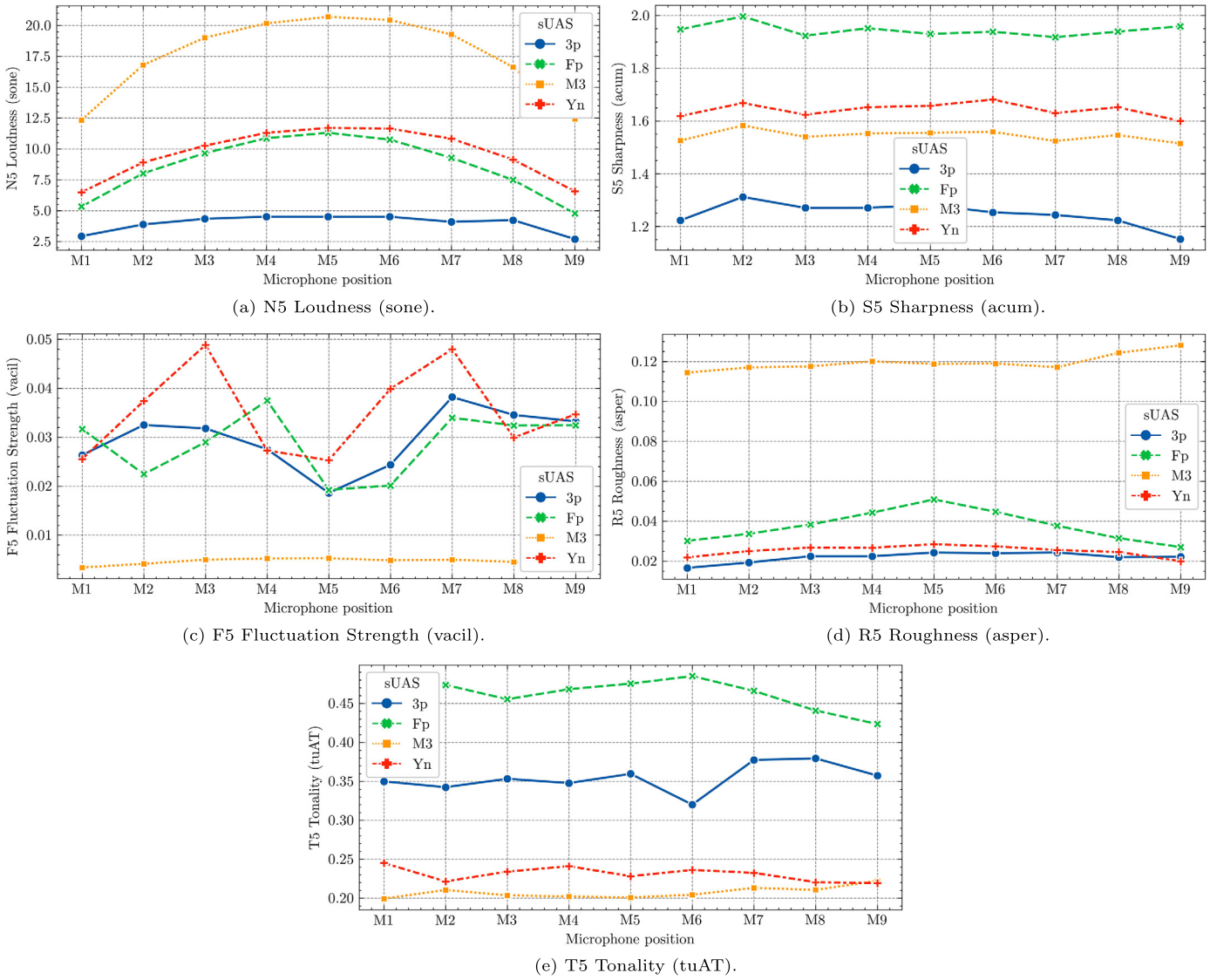

(a) N5 Loudness (sone).

(b) S5 Sharpness (acum).

(c) F5 Fluctuation Strength (vacil).

(d) R5 Roughness (asper).

(e) T5 Tonality (tuAT).

Fig. 16. Sound Quality Metrics 5^{th} percentile for four sUAS flying over the microphone line array at 15 m/s and $h_{AGL} = 10$ m. The 5^{th} percentile represents the loudness level below which 95% of the reported SQM values fall.

quency analysis (e.g., broadband vs. tonal noise). The method can be implemented for the acoustic characterisation of a variety of rotorcraft or multi-rotors varying in size, allowing enough signal-to-noise ratio for the computation of noise metrics. Under favourable weather conditions, the method has been proven to provide significant consistency in the acoustic metrics computed for a series of flyovers of the different sUAS tested.

Four different sUAS varying in size, number of rotors and blade count per rotor have been investigated. Changes in noise emission with varying payload and flyover speed have also been investigated. This paper has found broadband noise to be the dominant noise source at flyover operations for large sUAS; while smaller sUAS have a higher contribution of tonal noise to the OASPL. Moreover, the maximum noise radiation of all the sUAS tested is at the rear arc of polar directivity. The maximum radiation is found to be in ϕ angles as high as 40° to 60° for the hexacopter *Yn*. To ensure the generalisation of the results presented in this paper, an aerodynamic scaling of the acoustic metrics has been done using an average Advance Ratio ($\overline{J}$). It has been found that even a small reduction in $\overline{J}$ can lead to an increase in tonal noise.

A series of SQMs have also been calculated to expand the results with a psychoacoustic assessment of the sUAS tested. Larger sUAS produce higher values of Loudness, while smaller sUAS have significantly higher values of Tonality (than larger sUAS). Interestingly, 3 out of the 4 sUAS tested have shown a significant increase in Fluctuation Strength at Θ angles $\pm 30°$, which seems to be due to maximum radiation of amplitude modulated noise at these angles, based on existing literature. This phenomenon will be further investigated in dedicated future research.

The method presented provides a significant advance in the measurement and analysis methods for sUAS, but integrating acoustic, psychoacoustic and aerodynamic data. It is hoped that this research could contribute to the further development of guidance on sUAS noise, in terms of data processing and reporting.

Further investigation will focus on expanding the type and size range of aircraft for testing, and also on adapting the method to account for other operational procedures (i.e., hover, landing and take-off). In addition, more operating conditions will be tested to enlarge the range of aerodynamic conditions (e.g., in terms of Advance Ratio) to further investigate their effects on noise emission and psychoacoustic characteristics.

Funding

The authors C. Ramos-Romero, N. Green, and A.J. Torija Martinez would like to acknowledge the funding provided by the UK Engineering and Physical Sciences Research Council for the DroneNoise project (EP/V031848/1).

The author C. Asensio would like to acknowledge the funding provided by the Ministry of Universities of the Government of Spain in the framework of the State Programme to Develop, Attract and Retain Talent, State Mobility sub-programme of the State Plan for Scientific, Technical and Innovation Research 2021-2023.

CRediT authorship contribution statement

Carlos Ramos-Romero: Conceptualisation, Methodology, Coding, Formal analysis, Investigation, Data curation, Writing – original draft, Visualisation. Nathan Green: Conceptualisation, Methodology, Investigation, Writing – original draft, Writing – review. Antonio J. Torija: Conceptualisation, Formal analysis, Investigation, Writing – original draft, Writing – review & editing, Funding acquisition. César Asensio: Formal analysis, Investigation, Writing – original draft, Writing review.

Declaration of competing interest

The authors declare that they have no known competing financial interests or personal relationships that could have appeared to influence the work reported in this paper.

Data availability

The data is provided as a reference in the paper.

Acknowledgements

The Authors want to mention the valuable support provided by the partners during the noise measurement campaign. DTLX, for helping to organise the sUAS operators and access to the land where the measurement campaign was undertaken. Edinburgh Drone Company, for providing the sUAS during the test and the qualified pilot. Hayes McKenzie: Noise & Acoustic Consultants, for providing the equipment to measure meteorological conditions during the measurements.

References

[1] A.J. Torija, C. Clark, A psychoacoustic approach to building knowledge about human response to noise of unmanned aerial vehicles, Int. J. Environ. Res. Public Health 18 (2021) 682.
[2] FAA, Unmanned Aircraft System (UAS) or drone operations, https://www.faa.gov/hazmat/air_carriers/operations/drones, 2022. (Accessed 23 February 2023).
[3] EASA, Open category - civil drones, https://www.easa.europa.eu/en/domains/civil-drones/drones-regulatory-framework-background/open-category-civil-drones, 2023. (Accessed 23 February 2023).
[4] CAA, Rules and categories of drone flying, Flying in the Open category, https://www.caa.co.uk/drones/, 2023. (Accessed 23 February 2023).
[5] D. Floreano, R.J. Wood, Science, technology and the future of small autonomous drones, Nature 521 (2015) 460–466.
[6] A.W. Christian, R. Cabell, Initial investigation into the psychoacoustic properties of small unmanned aerial system noise, in: 23rd AIAA/CEAS Aeroacoustics Conference, 2017, p. 4051.
[7] D.Y. Gwak, D. Han, S. Lee, Sound quality factors influencing annoyance from hovering UAV, J. Sound Vib. 489 (2020) 115651.
[8] A.J. Torija, R.K. Nicholls, Investigation of metrics for assessing human response to drone noise, Int. J. Environ. Res. Public Health 19 (2022) 3152.
[9] B. Schäffer, R. Pieren, K. Heutschi, J.M. Wunderli, S. Becker, Drone noise emission characteristics and noise effects on humans—a systematic review, Int. J. Environ. Res. Public Health 18 (2021) 5940.
[10] R. Aalmoes, M. Tojal Castro, N. Sieben, R. Roosien, Drone noise in my backyard: the challenges for public acceptability, in: INTER-NOISE 2022 Congress, Institute of Noise Control Engineering, 2022.
[11] B. Schäffer, R. Pieren, K. Heutschi, J.M. Wunderli, S. Becker, Drone noise emission characteristics and noise effects on humans—a systematic review, Int. J. Environ. Res. Public Health 18 (2021) 5940.
[12] G. Sinibaldi, L. Marino, Experimental analysis on the noise of propellers for small UAV, Appl. Acoust. 74 (2013) 79–88.
[13] H. Wu, H. Jiang, P. Zhou, S. Zhong, X. Zhang, G. Zhou, B. Chen, On identifying the deterministic components of propeller noise, Aerosp. Sci. Technol. 130 (2022) 107948.
[14] H. Bu, H. Wu, C. Bertin, Y. Fang, S. Zhong, Aerodynamic and acoustic measurements of dual small-scale propellers, J. Sound Vib. 511 (2021) 116330.
[15] C.E. Tinney, J. Sirohi, Multirotor drone noise at static thrust, AIAA J. 56 (2018) 2816–2826.
[16] N. Zawodny, N. Pettingill, Acoustic wind tunnel measurements of a quadcopter in hover and forward flight conditions, in: INTER-NOISE and NOISE-CON Congress and Conference Proceedings, vol. 258, Institute of Noise Control Engineering, 2018, pp. 487–500.
[17] T. Zhou, H. Jiang, B. Huang, Quad-copter noise measurements under realistic flight conditions, Aerosp. Sci. Technol. 124 (2022) 107542.
[18] W.N. Alexander, J. Whelchel, N. Intaratep, A. Trani, Predicting community noise of sUAS, in: 25th AIAA/CEAS Aeroacoustics Conference, 2019, p. 2686.
[19] C.M. Hobbs, J. Page, T. Schultz, Acoustic repropagation technique and practical source characterization for simulation noise model databases, in: 24th National Conference on Noise Control Engineering 2010, Noise-Con 2010, Held Jointly with the 159th Meeting of the Acoustical Society of America, Baltimore, Maryland, USA, 2010, pp. 1166–1178.
[20] R.J. Higgins, A. Zarev, R.B. Green, G.N. Barakos, Investigation of a four-bladed propeller inflow at yaw, Aerosp. Sci. Technol. 124 (2022) 107530.
[21] D.Y. Gwak, D. Han, S. Lee, Sound quality factors influencing annoyance from hovering UAV, J. Sound Vib. 489 (2020) 115651.
[22] J.M. Wunderli, J. Meister, O. Boolakee, K. Heutschi, A method to measure and model acoustic emissions of multicopters, Int. J. Environ. Res. Public Health 20 (2023) 96.
[23] NASA-UNWG-Subgroup 2, UAM Ground & Flight Test Measurement Protocol, 2022. (Accessed 11 April 2022).
[24] Technical Committee: ISO/TC 20/SC 16 Unmanned aircraft systems, Noise measurements for UAS (unmanned aircraft systems), Draft International Standard, International Organization for Standardization, Geneva, Switzerland, 2023.
[25] W.M. Humphreys, D.P. Lockard, M.R. Khorrami, W. Culliton, R. McSwain, P.A. Ravetta, Z. Johns, Development and calibration of a field-deployable microphone phased array for propulsion and airframe noise flyover measurements, in: 22nd AIAA/CEAS Aeroacoustics Conference, 2016, p. 2898.
[26] Y. Zhang, I. Lee, D. Lin, Measurement of noise from a moving drone using a phased array microphone system, in: Proceedings of the 2017 Asia-Pacific International Symposium on Aerospace Technology, Seoul, Korea, 2017, pp. 16–18.
[27] I. Besnea, Acoustic imaging and spectral analysis for assessing UAV noise, https://matheo.uliege.be/handle/2268.2/13877, 2020, Delft University of Technology, Netherlands.
[28] N. Kloet, S. Watkins, R. Clothier, Acoustic signature measurement of small multi-rotor unmanned aircraft systems, Int. J. Micro Air Veh. 9 (2017) 3–14.
[29] K. Cussen, S. Garruccio, J. Kennedy, UAV noise emission - a combined experimental and numerical assessment, Acoustics 4 (2022) 297–312.
[30] A. Yehorova, E. Lumnitzer, Analysis of methodologies in the field of objective evaluation of acoustic drone descriptors, Acta Tech. Corvin. Bull. Eng. 14 (2021) 61–64.
[31] D.A. Senzig, M. Marsan, C.J. Cutler, D.R. Read, et al., Sound exposure level duration adjustments in UAS rotorcraft noise certification tests, Technical Report, John A. Volpe National Transportation Systems Center (US), Cambridge, MA, 2018, https://rosap.ntl.bts.gov/view/dot/37057.
[32] D. Senzig, M. Marsan, UAS noise certification, in: INTER-NOISE and NOISE-CON Congress and Conference Proceedings, vol. 258, Institute of Noise Control Engineering, 2018, pp. 3718–3726, https://rosap.ntl.bts.gov/view/dot/36817.
[33] D.R. Read, D.A. Senzig, C.J. Cutler, E. Elmore, H. He, et al., Noise Measurement Report: Unconventional Aircraft-Choctaw Nation of Oklahoma: July 2019, Technical Report, John A. Volpe National Transportation Systems Center, Cambridge, MA, 2020, https://rosap.ntl.bts.gov/view/dot/49647.
[34] A.W. Christian, R. Cabell, Initial investigation into the psychoacoustic properties of small unmanned aerial system noise, in: 23rd AIAA/CEAS Aeroacoustics Conference, 2017, p. 4051, NF1676L-25753.
[35] N.S. Zawodny, A. Christian, R. Cabell, A summary of NASA research exploring the acoustics of small unmanned aerial systems, in: 2018 AHS Technical Meeting on Aeromechanics Design for Transformative Vertical Flight, 2018, p. 11, NF1676L-27827.
[36] W.N. Alexander, J. Whelchel, Flyover noise of multi-rotor sUAS, in: Inter-Noise and Noise-Con Congress and Conference Proceedings, vol. 7, Institute of Noise Control Engineering, 2019, pp. 2548–2558, http://www.sea-acustica.es/fileadmin/INTERNOISE_2019/Enter.htm.
[37] V. Didkovskyi, O. Korzhyk, S. Kozeruk, A. Kozak, R. Kostiuk, S. Liakhevych, Noise measurement of the multicopter UAV, in: 2019 IEEE 5th International Conference Actual Problems of Unmanned Aerial Vehicles Developments (APUAVD), IEEE, 2019, pp. 67–70.

[38] G. Beaulieu, Master thesis and internship: Experimental procedure for measuring the noise annoyance from multi-rotor maneuvers using a UAV system, https://matheo.uliege.be/handle/2268.2/13877, 2022, Université de Liège, Liège, Belgique.
[39] C.J. Hui, M.J. Kingan, Y. Hioka, G. Schmid, G. Dodd, K.N. Dirks, S. Edlin, S. Mascarenhas, Y.-M. Shim, Quantification of the psychoacoustic effect of noise from small unmanned aerial vehicles, Int. J. Environ. Res. Public Health 18 (2021) 8893.
[40] C. Cutler-Wood, M. Barzach, R. Downs, C. Hobbs, S. Shirayama, Estimating unmanned aircraft takeoff noise using hover measurement data, in: QUIET DRONES Second International Symposium on Noise from UASs/UAVs and eVTOLs, iNCEEurope, Centre d'information sur le Bruit, Paris, France, 2022, p. 13, https://rosap.ntl.bts.gov/view/dot/64152.
[41] N.B. Konzel, E. Greenwood, Ground-based acoustic measurements of small multirotor aircraft, in: Vertical Flight Society's 78th Annual Forum & Technology Display, Vertical Flight Society, 2022, p. 11.
[42] EASA, Guidelines on noise measurement of unmanned aircraft systems lighter than 600 kg. Operating in the specific category (low and medium risk), Public consultation, https://www.easa.europa.eu/en/downloads/137139/en, 2022. (Accessed 23 February 2023).
[43] R. Cabell, F. Grosveld, R. McSwain, Measured noise from small unmanned aerial vehicles, in: Inter-Noise and Noise-Con Congress and Conference Proceedings, vol. 252, Institute of Noise Control Engineering, 2016, pp. 345–354, NF1676L-23558.
[44] C. Ramos-Romero, N. Green, C. Asensio, A.J. Torija, DroneNoise Database, acoustics and psychoacoustics metrics database from EPSRC DroneNoise Project EP/V031848/1, Acoustics Research Centre - University of Salford, 2023, https://doi.org/10.17866/rd.salford.22133411.
[45] EASA, Research project report - rotorcraft noise modelling method by Netherlands Aerospace Centre (NLR), https://www.easa.europa.eu/en/research-projects/environmental-research-rotorcraft-noise, 2015. (Accessed 23 February 2023).
[46] M.C. Anderson, J.H. Stephenson, N.S. Zawodny, K.L. Gee, Characterizing the effects of two ground-based outdoor microphone configurations, in: Proceedings of Meetings on Acoustics 178th ASA, vol. 39, Acoustical Society of America, 2019, 055011.
[47] P. Rasmussen, L. Lars Winberg, Accurate measurement of drone noise on the ground, in: QUIET DRONES Second International Symposium on Noise from UASs/UAVs and eVTOLs, INCEEurope, Centre d'information sur le Bruit, Paris, France, 2022, p. 11.
[48] ICAO, Annex 16 to the Convention on International Civil Aviation. International Standards and Recommended Practices. Environmental Protection. Aircraft Noise, 2017.
[49] W.L. Willshire Jr., P.A. Nystrom, Investigation of effects of microphone position and orientation on near-ground noise measurements, Technical Report, NASA Langley Research Center, Hampton, VA, 1982, NASA technical paper TS-2004.
[50] ICAO, Environmental Technical Manual. Procedures for the Noise Certification of Aircraft, 2015.
[51] K. Jones, R. Cadoux, Metrics for aircraft noise, ERCD Report 0904, 2009.
[52] S. Min, D. Lim, D.N. Mavris, Aircraft noise reduction technology and airport noise analysis for general aviation revitalization, in: 15th AIAA Aviation Technology, Integration, and Operations Conference, 2015, p. 2389.
[53] ISO 9613-2:1996, Acoustics – attenuation of sound during propagation outdoors – Part 2: General method of calculation, Standard, International Organization for Standardization, Geneva, Switzerland, 1996.
[54] C.H. Hansen, Fundamentals of acoustics, in: Occupational Exposure to Noise: Evaluation, Prevention and Control, vol. 1, World Health Organization, 2001, pp. 23–52.
[55] L.E. Kinsler, A.R. Frey, A.B. Coppens, J.V. Sanders, Fundamentals of Acoustics, John Wiley & Sons, 2000.
[56] R. Kapoor, N. Kloet, A. Gardi, A. Mohamed, R. Sabatini, Sound propagation modelling for manned and unmanned aircraft noise assessment and mitigation: a review, Atmosphere 12 (2021) 1424.
[57] K. Attenborough, Sound Propagation in the Atmosphere, Springer, New York, New York, NY, 2007.
[58] F. Mobley, B. Davis, J. Hall, T. Moore, Decontamination of acoustic measurement with critical point noise detection, Appl. Acoust. 138 (2018) 156–162.
[59] H.E. Bass, L.C. Sutherland, A.J. Zuckerwar, D.T. Blackstock, D. Hester, Atmospheric absorption of sound: Further developments, J. Acoust. Soc. Am. 97 (1995) 680–683.
[60] ISO 9613-1:1993, Acoustics – attenuation of sound during propagation outdoors – Part 1: Calculation of the absorption of sound by the atmosphere, Standard, International Organization for Standardization, Geneva, Switzerland, 1993.
[61] F. Mobley, S. Campbell, Validation of acoustic directivity patterns from static and dynamic flight measurements, in: INTER-NOISE and NOISE-CON Congress and Conference Proceedings, vol. 264, Institute of Noise Control Engineering, 2022, pp. 174–187.
[62] Y. Fuerkaiti, E. Grande, D. Casalino, F. Avallone, D. Ragni, Efficient low-fidelity aeroacoustic permanence calculation of propellers, Aerosp. Sci. Technol. 123 (2022) 107438.
[63] J.V. Foster, D. Hartman, High-fidelity multi-rotor unmanned aircraft system (UAS) simulation development for trajectory prediction under off-nominal flight dynamics, in: 17th AIAA Aviation Technology, Integration, and Operations Conference, 2017, p. 3271.
[64] I. Djurek, A. Petosic, S. Grubesa, M. Suhanek, Analysis of a quadcopter's acoustic signature in different flight regimes, IEEE Access 8 (2020) 10662–10670.
[65] K. Heutschi, B. Ott, T. Nussbaumer, P. Wellig, Synthesis of real world drone signals based on lab recordings, Acta Acust. 4 (2020) 24.
[66] F. Casagrande Hirono, A. Torija Martinez, A. Elliott, Optimization of a contra-rotating propeller rig for reduced psychoacoustic impact, in: INTER-NOISE and NOISE-CON Congress and Conference Proceedings, vol. 265, Institute of Noise Control Engineering, 2023, pp. 4077–4087.
[67] A.R. Aumann, B.C. Tuttle, W.L. Chapin, S.A. Rizzi, The NASA Auralization Framework and plugin architecture, in: Inter-Noise and Noise-Con Congress and Conference Proceedings, Institute of Noise Control Engineering, 2015, pp. 2825–2836, https://ntrs.nasa.gov/citations/20160006430.
[68] J.M. Wunderli, R. Pieren, M. Habermacher, D. Vienneau, C. Cajochen, N. Probst-Hensch, M. Röösli, M. Brink, Intermittency ratio: a metric reflecting short-term temporal variations of transportation noise exposure, J. Expo. Sci. Environ. Epidemiol. 26 (2016) 575–585.
[69] C.A. Authority, The noise and number index, ERCD7907, 1981.
[70] C. Asensio, I. Pavón, M. Ruiz, R. Pagan, M. Recuero, Estimation of directivity and sound power levels emitted by aircrafts during taxiing, for outdoor noise prediction purpose, Appl. Acoust. 68 (2007) 1263–1279.
[71] S.A. Rizzi, D.L. Huff, D.D. Boyd, P. Bent, B.S. Henderson, K.A. Pascioni, D.C. Sargent, D.L. Josephson, M. Marsan, H.B. He, et al., Urban air mobility noise: current practice, gaps, and recommendations, Technical Report, National Aeronautics and Space Administration, Langley Research Center, Hampton, Virginia, 2020, NASA/TP-2020-5007433.
[72] A.J. Torija, R.H. Self, J.L. Lawrence, Psychoacoustic characterisation of a small fixed-pitch quadcopter, in: Inter-Noise and Noise-Con Congress and Conference Proceedings, vol. 259, Institute of Noise Control Engineering, 2019, pp. 1884–1894, http://usir.salford.ac.uk/id/eprint/53243/.
[73] E.I. Greenwood, F.H. Schmitz, Separation of main and tail rotor noise sources from ground-based acoustic measurements using time-domain dedopplerization, in: 35th European Rotorcraft Forum 2009, 2009, LF99-9186.
[74] H. Bian, Q. Tan, S. Zhong, X. Zhang, Reprint of: Assessment of UAM and drone noise impact on the environment based on virtual flights, Aerosp. Sci. Technol. 125 (2022) 107547.
[75] Head Acoustics, Loudness and sharpness calculation, in: Psychoacoustic Analyses I, HEAD Acoustics, 2018.
[76] Head Acoustics, Calculating psychoacoustic parameters in ArtemiS SUITE, in: Psychoacoustic Analyses II, HEAD Acoustics, 2018.
[77] S. Krishnamurthy, M.A. Boucher, A.W. Christian, S.A. Rizzi, Rotorcraft sound quality metric test 1: Stimuli generation and supplemental analyses, NTRS - NASA Technical Reports Server, 2021, NASA/TM-20205008997.
[78] M.A. Boucher, S. Krishnamurthy, A.W. Christian, S.A. Rizzi, Sound quality metric indicators of rotorcraft noise annoyance using multilevel analysis, J. Acoust. Soc. Am. 153 (2023) 867–876.
[79] A.J. Torija, R.K. Nicholls, Investigation of metrics for assessing human response to drone noise, Int. J. Environ. Res. Public Health 19 (2022) 3152.
[80] D. Read, C. Roof, et al., Research to support new entrants to public airspace and aircraft noise certification, INCEEurope, Centre d'information sur le Bruit, 2020, p. 17.
[81] J. Treichl, S. Körper, Untersuchung der geräuschemission von drohnen/investigation of the noise emission of drones, Lärmbekämpfung 14 (2019) 108–114.
[82] H. Fastl, E. Zwicker, Psychoacoustics: Facts and Models, vol. 22, Springer Science & Business Media, 2006.
[83] W.J. Baars, L. Bullard, A. Mohamed, Quantifying modulation in the acoustic field of a small-scale rotor using bispectral analysis, in: AIAA Scitech 2021 Forum, 2021, p. 0713.
[84] A.J. Torija, P. Chaitanya, Z. Li, Psychoacoustic analysis of contra-rotating propeller noise for unmanned aerial vehicles, J. Acoust. Soc. Am. 149 (2021) 835–846.
[85] A.J. Torija, Z. Li, P. Chaitanya, Psychoacoustic modelling of rotor noise, J. Acoust. Soc. Am. 151 (2022) 1804–1815.